

Laser surface alloying of copper with titanium: Part I.

Electrical wear resistance in dry condition

C.T. Kwok^{a,b}, P.K. Wong^a, H.C. Man^c

^a Department of Electromechanical Engineering, University of Macau, China

^b Institute of Applied Physics and Materials Engineering, University of Macau, China

^c Department of Industrial and Systems Engineering, The Hong Kong Polytechnic

University, Hong Kong, China

Abstract

A high-power diode laser was used for alloying titanium on commercially pure copper (cp Cu) for enhancing electrical sliding wear in air. Microstructure and phases present were analyzed using scanning-electron microscopy and X-ray diffraction, respectively. Electrical sliding wear tests in air were conducted with a pin-on-disc tribometer with and without electric current. The electrical sliding wear resistances of all laser-alloyed samples are significantly enhanced by 3 orders of magnitude as compared with cp Cu. Among the laser-alloyed samples, the one with 70 wt% Ti and average hardness of 661 HV_{0.2} possesses the highest electrical sliding wear resistance. The enhancement in electrical wear resistance in air is attributed to the presence of Cu-Ti intermetallic phases (IMP) and solid solution hardening.

Keywords: laser surface alloying; intermetallic phases; hardness; electrical sliding wear

1. Introduction

Copper (Cu) and its alloys are widely applied as electric contacts materials, such as overhead contact wires, commutators, electronic devices, lead frame materials for

integrated circuits [1, 2] due to excellent electrical and thermal conductivities, a combination of strength and ductility, and good fatigue resistance [3-6]. However, their major drawbacks are low hardness, low softening temperature and low resistance to wear [7]. These drawbacks have attracted research attention in fabricating a surface layer on Cu for improving the wear resistance while retaining its bulk properties. On the other hand, copper-titanium (Cu-Ti) intermetallic compounds are very hard, and good electric conductors and sound absorbers [8-10]. From the Cu-Ti binary phase diagram, it can be noticed that various kinds of intermetallic phases can be formed [11, 12]. However, the positions of Cu and Ti in the electromotive force series indicate that coating of Cu with Ti by conventional electroplating is not possible. Thus, coatings of Cu-Ti are normally produced by physical vapor deposition or pack cementation methods [13, 14]. However, the limitations of these methods include requirement of vacuum and high temperature environments. These kinds of coatings are fabricated in a chamber or a furnace. Thus the size of the workpiece is restricted. In the present study, laser surface alloying (LSA) was adopted to fabricate Cu-Ti coatings on pure Cu with a high power diode laser (HPDL). LSA is a technique that involves melting of a thin layer of the underlying substrate and a pre-deposited or co-deposited layer of alloying materials to form an alloyed zone on the surface by rapid solidification. With the addition of alloying element(s) and rapid solidification, a tailor-made surface which is not achievable by other techniques in ambient environment could be produced. Due to high precision and efficiency, localized thermal action and power controllability of a laser beam [15-17], LSA has been widely applied in manufacturing surface coatings for improving wear, corrosion and oxidation resistances while retaining the bulk properties such as mechanical strength and conductivity of the substrate [9, 17, 18-21]. Owing to the high reflectivity of Cu to near infra-red laser and high thermal conductivity, studies on LSA of pure Cu are scarcely reported. Guo

and his co-workers [9] synthesized coatings of Ti-Cu intermetallic compounds on pure Ti substrate by laser cladding and their tribological properties were studied. It was reported that the wear rate of the Ti-Cu coating decreased with increasing sliding speed from 0.05 to 0.2 m/s, while the wear rate increased with normal load from 5 N to 15 N. However, the normal load and sliding speed for the laser-clad Ti-Cu on Ti substrate are quite low as compared with the operating conditions of some high-speed applications such as current collectors of the railway systems and commutators. In the present study, the electrical sliding wear behavior of the laser-alloyed Cu-Ti layers in dry condition (in air) was evaluated in Part I while the electrical sliding wear behavior in wet and corrosive environment will be reported in Part II [22].

2. Experimental details

Commercially pure copper (cp Cu) rectangular plates with dimensions of 22 mm x 19 mm x 6.3 mm were used as the substrate. To increase the surface roughness of the substrate for better adhesion with the preplaced pure Ti powder (International Laboratory, 99%) as well as removing the surface oxides, the cp Cu plates were ground with 80-grit SiC paper. The Ti powder with size of 4.4 μm was mixed with 4 wt.% polyvinyl alcohol and the slurry of Ti powder was then pasted onto cp Cu with a thickness of about 0.15 mm. To improve the absorptivity of cp Cu with the laser energy [19, 23-25], the Ti powder was preplaced onto the substrate instead of spraying with an in-situ nozzle. The samples were preheated to 200 °C to reduce the residual tensile stress and prevent microcracks which lead to disconnection of the coating to the substrate [26]. LSA was subsequently carried out using a 2.3-kW CW high-power diode laser (HPDL) module (Laserline, LDM 1000-1000) at a power of 2 kW, a beam diameter of 2 mm and scanning speeds ranging from 20 to 35 mm/s. With the short wavelength (990 nm), HPDL is better absorbed by the metallic materials. To prevent

from oxidation during the LSA process, Argon gas was used as the shielding gas and the flow rate was controlled to be 15 L/min. The melt surface was produced by 50% overlapping of consecutive parallel melt tracks. Single preplaced Ti layer for LSA was found to have a high degree of dilution in the alloyed zone, thus a second Ti layer with the same thickness was preplaced on the previously laser-alloyed samples. LSA was then carried out with the same processing conditions as the first layer to increase the coating thickness. The degree of dilution of the laser-alloyed layers is known as the dilution ratio (DR) and is defined in equation (1):

$$DR = \left(1 - \frac{2t}{D}\right) \times 100 \% \quad (1)$$

where t is the preplaced coating thickness per layer and D is thickness of the alloyed layers.

After LSA, microstructural and compositional analyses were performed using a scanning-electron microscope (SEM, Hitachi S-3400N) equipped with an energy dispersive X-ray spectrometer (EDS, Horiba EX-250) for analyzing the surface and cross-section of the laser-alloyed samples. Phase identification was conducted using a X-ray diffractometer (XRD, Rigaku MiniFlex 600) with $\text{CuK}\alpha$ radiation operating at 40 kV and 15 mA and the scan rate was 0.1 °/s. Transmission electron microscopy (TEM, Jeol JEM 2010F) was used to examine the dislocations in the laser-alloyed layers before and after wear test.

The hardness profiles along the depths of the laser-alloyed layers as well as the hardness of the worn surface after electrical sliding wear tests were measured by means of a microhardness tester with a load of 200 g and a dwell time of 10 s. As the thicknesses of the laser-alloyed specimens after electrical sliding wear tests were larger than 0.1 mm, a load of 200 g still would not incur substrate effect in hardness measurement. Five different locations were selected for the hardness measurement and the average hardness values were obtained.

Electrical sliding wear testing was conducted using a pin-on-disc tribometer as shown in Fig. 1. The disc with diameter of 420 mm and thickness of 12 mm was attached to a spindle driven by a 7.5-kW variable-frequency high-speed electrical motor. The electric current applied on the specimens (the pins) was provided by a DC power supply as the anode. A normal load of 50 N was applied to the samples for maintaining the contact with the disc by a hydraulic press. The samples were forced to slide against a counterface tool steel rotating disc with hardness of 600 HV_{0.2}. In a third rail system, Cu is used as the current collector shoes and steel is used as the third rail for providing electric power. Moreover, the iron-base contact strips (pantograph) were used in some catenary systems [14]. The wear tests were conducted at a constant load of 50 N, and sliding speed of 60 km/h, without and with DC current (60 A) in dry condition (in air). In dry condition, the tests were conducted at ambient temperature (25 °C) and a relative humidity of 60%. During the electrical sliding wear test, the weight loss ΔW (in g) of the samples was intermittently recorded at a time interval of 1 minute (for sliding at 60 km/h) or 1.5 minute (for sliding at 40 km/h) using an electronic balance with an accuracy of ± 0.1 mg. All the tests were repeated three times to ensure the repeatability of the experimental data at the same testing conditions. The average wear (thickness) loss (Δd) was then calculated by:

$$\Delta d \text{ (mm)} = 10 \frac{\Delta W}{\rho A} \quad (2)$$

where ρ (in g/cm³) and A (in cm²) are the density and the exposed surface area of cp Cu or the laser-alloyed layers respectively. The densities of the laser-alloyed layers were calculated according to the weight fractions of Cu and Ti (Table 1) by the rule of mixture:

$$\rho = \left(\frac{W_{Cu}}{\rho_{Cu}} + \frac{W_{Ti}}{\rho_{Ti}} \right)^{-1} \quad (3)$$

where $\rho_{Cu} = 8.9$ g/cm³ and $\rho_{Ti} = 4.5$ g/cm³ are the theoretical densities of Cu and Ti

respectively, and the corresponding weight fractions of Cu and Ti in the laser-fabricated Ti-Cu layer are W_{Cu} and W_{Ti} respectively ($W_{Cu} = 1 - W_{Ti}$).

The average rates of wear loss of materials are expressed in terms of the wear rate in dry condition (D) and calculated by the following equation:

$$\text{Wear rate (mm/h)} = \frac{\Delta d}{\Delta t} \quad (4)$$

where Δt (in h) is the duration of the wear test.

After electrical sliding wear tests, the worn surface and debris from the samples were analysed using a SEM equipped with EDX, and XRD.

3. Results and discussion

3.1 Microstructure

The laser parameters, compositions, phase present and coating thickness of the laser-alloyed samples are summarized in Table 1. The laser-alloyed samples are designated as LA-Ti-Cu-XX where XX denotes the scanning speeds of the laser beam (20, 25, 30 and 35 mm/s). Detailed microstructural analysis for the laser-alloyed cp Cu with Ti fabricated at various scanning speeds has been reported in a previous study of the present authors [18]. Typical cross-sectional view and microstructure of the laser-alloyed samples LA-Ti-Cu-30 revealing fine dendritic structure are shown in Fig. 2(a-b). The alloyed layers are metallurgically bonded to the cp Cu substrate without cracks and porosities. No microcracks are also observed around the indent mark at the interface of the substrate and the laser-alloyed IMP layer after Vickers hardness test (Fig. 2(c)). Moreover, no visible detachment of the laser-alloyed layer from the substrate is seen due to the strong metallurgical bond formed between the laser-alloyed layer and the substrate. Cracking at the coating-substrate interface is a common problem in coatings [27]. The present result is consistent with the finding of Franco et al. [27], who reported that no microcrack and no major coating detachment

were seen along the interface between the as-deposited Ni–P/SiC coatings and aluminum alloy substrate. However, the heat-treated Ni–P/SiC coatings were found to be more brittle and microcracks were observed along the interface especially at higher load owing to the difference in thermal expansion and contraction occurring at the interface. In the present study, the difference in coefficients of the thermal expansion of Cu and Ti is small. Hence, the effect of thermal expansion and contraction due to rapid solidification in LSA process is less pronounced.

When the sample was irradiated by the laser beam, the preplaced Ti powder absorbed the laser energy and melting of the Ti powder occurred immediately. Heat was transferred to the substrate via convection and conduction of the molten pool. Due to thermal gradient and surface tension, Marangoni convection promoted mixing of the molten metal. Dendrites were formed in the molten pool owing to constitutional supercooling during solidification. The solidification rate was lowest near the interface and increased when moving inward to the molten pool. Since there was no preferred heat flow direction at the center of the molten pool, dendritic growth was random as shown in Fig 2(b).

For the laser-alloyed samples with the same preplaced thickness of Ti layer fabricated at fixed energy density, the Ti content increased (or Cu content decreases) with the increase in the scanning speed ranging from 20 to 35 mm/s. At the scanning speed higher than 35 mm/s, the deliverable energy density was reduced and was insufficient to melt the thicker Ti powder layer. From Table 1, the dilution ratio (degree of dilution) and thickness of the alloyed layers increased as the laser scanning speed decreased. The thicknesses of the alloyed layers fabricated at laser scanning speeds of 35 - 20 mm/s ranged from 0.35 - 0.8 mm. From the XRD patterns shown in Fig. 3, the surface of the alloyed layers was composed of different Cu-Ti intermetallic phases (IMPs) (CuTi_2 , CuTi , Cu_4Ti_3 , Cu_4Ti) and metallic phases (fcc α -Cu and hcp

α -Ti) as summarized in Table 1 [18]. The alloyed layers fabricated at higher speeds, i.e. 25, 30 and 35 mm/s, were composed of Ti-rich IMP (CuTi_2) as the major phase. On the other hand, α -Cu and Cu-rich IMP (Cu_4Ti) were detected for the sample LA-Ti-Cu-20 (with 25 wt% Ti) fabricated at lower speed, i.e. 20 mm/s because longer interaction promoted mixing of more molten Cu from the substrate with Ti. High Cu content in the alloyed layer would favor the formation of α -Cu and Cu-rich IMP (Cu_4Ti) according to the binary phase diagram of Cu-Ti system [12]. The laser-alloyed samples fabricated at various scanning speeds of 20, 25, 30 and 35 mm/s had average Ti contents of 25 wt.%, 50 wt.%, 70 wt.% and 85 wt.%, respectively. Cao et al [28] reported that in the solidification process, CuTi_2 phase with melting temperature of 1005 °C nucleated and grew first. As the temperature and Ti content decreased, CuTi phase with a lower melting temperature of 982 °C nucleated and grew. Microstructural examinations revealed that CuTi_2 was the major phase formed in alloyed layers fabricated at scanning speeds of 25, 30 and 35 mm/s. Minor peaks of other IMPs (CuTi , Cu_4Ti_3 and Cu_4Ti) were detected as the temperature and Ti content started diminishing. XRD patterns of LA-Cu-Ti-20 show that α -Cu has the highest intensity peak and minor peaks of Cu_4Ti are also present. This indicates that the degree of dilution of Ti is high and α -Cu is the major phase present [18].

3.2 Hardness

Fig. 4 shows the hardness profiles of the laser-alloyed samples fabricated at various laser scanning speeds. The hardness in the alloyed zones of the samples is uniform and the average hardness values are extracted as shown in Table 2. It can be observed that LA-Cu-Ti-30 has the highest hardness (661 $\text{HV}_{0.2}$) and is about 8.8 times that of cp Cu (75 $\text{HV}_{0.2}$). The enhanced hardness is attributed to solid solution strengthening and existence of Cu-Ti intermetallic phases in the laser-alloyed layers.

LA-Cu-Ti-35 and LA-Cu-Ti-20 has a lower hardness of 541 HV_{0.2} and 362 HV_{0.2} respectively due to the presence of softer metallic phases (α -Ti for the former and α -Cu for the latter).

3.3 Electrical sliding wear behavior in dry condition

The cumulative thickness loss against distance traveled of various laser-alloyed samples worn at 60 km/h without and with a DC current in dry condition are shown in Fig. 5(a-b). The values of wear rate are shown in Table 3 and the plot of wear rates of various samples are depicted in Fig. 5(c). Indeed, all wear rates of the laser-alloyed specimens are much lower than that of cp Cu indicating the Cu-Ti IMPs are crucial for enhancing electrical wear resistance. The ranking of electrical wear resistance (defined as the reciprocal of wear rate, in h/mm) of various laser-alloyed specimens at 60 km/h and 60 A is:

$$\text{LA-Ti-Cu-30} > \text{LA-Ti-Cu-35} \sim \text{LA-Ti-Cu-25} > \text{LA-Ti-Cu-20} \gg \text{cp Cu}$$

3.3.1 Effect of sliding speed and current intensity

The wear rate increases with the presence of electric current and increase in sliding speed (Fig. 5(a-b) and Table 3). Without electric current, the material loss is attributed to the plastic deformation and frictional heating. The actual loss rate with current was considered to be including both damage mechanisms, namely: (i) mechanical wear (or dynamic erosion) (adhesion/abrasion/oxidation) and (ii) arc erosion (static erosion), which includes splash erosion and vaporization. In dry sliding at high speed, the shearing and ploughing in the sliding contact will be so rapid that the frictional heat will be generated much faster than the heat can be conducted away [9]. The temperature rise leads to a reduction in hardness and higher wear rate, according to the Archard's equation:

$$\text{Wear rate} = \frac{kFv}{H} \quad (5)$$

where k is the wear coefficient, F is the normal force, v is the sliding speed and H is the hardness of the material. It was reported that the surface temperature of the sliding surface of Cu sliding against chrome steel could increase to 600 °C under an electric field [29]. Consequently, the heat dissipated by the applied current further intensifies the Joule heating effect in the sliding system and results in higher wear rate. Besides, the presence of electric current in the sliding system results in electric arcing. Contact arcing gives rise to arc erosion and arc heating causing material loss. Jia et al. [30] reported that Joule heating caused by electric current and arc heating made a significant contribution to the wear rate of Cu-Ag-Cr alloy as the temperature of the arc plasma could reach 3200 – 3700 °C. Arc melting and arc erosion will occur [30-32]. Electrical sliding wear phenomena depend on the polarity in air [33, 34]. Oxidation wear dominates when the sample is anode, and changes to abrasive wear when the polarity is changed to cathode. In the present study, the laser-alloyed specimens or cp Cu were the anodes, sliding against the counterface steel disc (the cathode) in air. Oxidation will also be more pronounced for sliding specimens in the presence of oxygen. When the oxide layer reaches a critical depth, it will be detached from the specimen surface by mechanical abrasion. When the counterface steel disc is cathode, oxidation will occur on the disc and iron oxides which act as hard abrasive may lead to abrasive wear.

3.3.2 Dry wear of cp Cu

For electrical sliding wear of cp Cu in air, the wear rate is very high (up to 293 mm/h at 60 km/h and 60 A). When cp Cu reached the softening temperature from frictional heat and Joule heating, cp Cu would be softened and catastrophic failure consequently arose. Massive metal transfer occurred and Cu-rich adhesive patches

were found on the counterface steel disc and this revealed adhesive wear. It is reported that the presence of oxide film on the surface of pure metals can act as a solid lubricant and also as an electrical insulator which is an important effect on separating the sliding surfaces [35, 36]. With the increase in the sliding distance, the oxide film penetrates into the metal surface and adhesion occurred at the interface [35, 36]. Copper oxide formed at the beginning of the electrical sliding wear test acts as a lubricant to avoid material loss. However, when the oxide layer breaks and when the softening temperature has been reached, pronounced adhesive wear will occur. In addition to the adhesive wear, when the oxide film reaches a critical thickness, it becomes unstable and breaks up [33, 37]. The detached copper oxide and the oxidized adhesive patches found on the counterface steel disc are harder than Cu. They will act as hard abrasives which causes abrasive wear. Thus, abrasive and adhesive wear of cp Cu are the dominant wear mechanisms in air.

3.3.3 Dry wear of laser-alloyed specimens

It is interesting that the electrical sliding wear rate of the sample LA-Ti-Cu-30 tested at 60 km/h and 60 A under dry condition is the lowest among the laser-alloyed samples [Fig. 5(c)]. LA-Ti-Cu-30 is the hardest among all the samples and the wear rate tends to decrease with higher hardness and higher content of Ti-rich IMPs (Table 1). The enhancement in electrical wear resistance is due to the combined effect of hard IMPs and solid solution strengthening after LSA. LA-Ti-Cu-30 consisted of high volume fraction of Ti-rich IMPs and the hardness was 660 HV_{0.2}, which is about 8.8 times that of cp Cu. It can be perceived that LA-Ti-Cu-35 (541 HV_{0.2}) is not as hard as LA-Ti-Cu-30 (660 HV_{0.2}) because of the higher Ti content (more α -Ti phase) in the former, as evidenced by the existence of α -Ti peaks in the XRD patterns as shown in Fig. 3(d). The hard IMPs can reduce the amount of transferred load to the Cu binder,

causing the applied load to be withstood mainly by the laser-alloyed layers [35]. The contact area between the samples and the counterface was reduced and thus sliding only occurred on very limited asperities and subsequently plastic deformation of the alloyed layers could be highly reduced [35]. In addition, the intrinsic non-stoichiometric properties of IMP coatings and adsorption of oxygen might cause the formation of surface oxide which acted as lubricant and could effectively reduce the wear loss [35, 38].

In the present study, two kinds of solid solutions have been formed during LSA with different laser scanning speeds, namely Cu-rich α -Cu (for LA-Ti-Cu-20 and LA-Ti-Cu-25) and Ti-rich α -Ti (for LA-Ti-Cu-30 and LA-Ti-Cu-35). Lattice strain imposed by the solute atoms (Cu and Ti) with different atomic radii (0.128 and 0.145 nm respectively) will hinder motion of dislocations and hence increase the strength of the alloyed layers. The hardness of Cu-rich α -Cu solid solution (4 at.% Ti) is reported to be about three times higher than that of copper substrate [39]. In addition to solid solution strengthening (α -Cu alloyed with Ti), the hardness of LA-Ti-Cu-20 was increased by 4.8 times due to existence of the minor phase Cu_4Ti . Moreover, Ohkubo et al. [40] reported that alloying Cu (3 to 5 wt.%) to Ti may reduce the stacking fault energy and give rise to higher wear resistance. However, these effects are less significant than that of the hard IMPs.

Besides the combined effect of hard Cu-Ti IMPs and solid solution strengthening after LSA, the effects of dislocation strengthening, particle strengthening (oxide particles), and composite strengthening (pick up of counter material or wear particles) during electrical sliding wear can also help to strengthen the laser-alloyed layers [41, 42]. From the TEM micrographs obtained from the surface of LA-Ti-Cu-30 before and after electrical sliding wear test (Fig. 6), it can be observed that the dislocation density of LA-Ti-Cu-30 at the Ti-rich solid solution significantly increased after

electrical sliding wear. This provides the evidence of dislocation strengthening causing increase in electrical sliding wear resistance of the laser-alloyed layers. Furthermore, the hardness of the worn surface of the laser-alloyed samples after wear test in dry condition is noticeably higher than that before wear tests as shown in Table 2. The harder worn surface is due to dislocation strengthening (work hardening) during the electrical sliding wear. Similar result was reported by Gao et al. [43]. After dry sliding wear test, the surface hardness of the laser melted/deposited Ti₂Ni/TiNi intermetallic alloy increased from 310 to 420 HV, showing strong work hardening effect by shear plastic deformation of the surface.

The worn surface and the cross-section of the laser-alloyed samples LA-Ti-Cu-20 and LA-Ti-Cu-30 after sliding at 60 km/h and 60 A in dry are shown in Fig. 7. After electrical sliding wear test in dry condition, the thickness of LA-Ti-Cu-30 was reduced from 0.4 mm to the range of 0.14 mm, whereas the thickness of LA-Ti-Cu-20 was reduced from 0.8 mm to the range of 0.32 mm. After the wear test, the susceptibility to cracking for the samples worn in air are listed in Table 2. No crack was observed in LA-Ti-Cu-20 (with lower hardness but higher ductility) as shown in Fig. 7(a)(i). On the other hand, surface cracks were found at the alloyed layers of samples with high fraction of hard but brittle IMPs, including LA-Ti-Cu-25, LA-Ti-Cu-30 and LA-Ti-Cu-35. As an example, the cracked alloyed layer in LA-Ti-Cu-30 is shown in Fig. 7(b). The cracking susceptibility of the laser-alloyed samples increased with increasing laser scanning speed (Table 2) due to the presence of more hard and brittle IMPs. Franco et al. reported that only shallow microcracks were seen near the surface of the electroless Ni-P/SiC composite coating (dry wear at 2 N and 200 °C), just about 2 μm beneath the wear track near to the stress concentrated region as compared with the SiC-free coating with wider and deeper wear damage [44]. For the composite coating with the SiC particles in the Ni-P matrix,

propagation of any crack formed was suppressed. As the probability for the crack to encounter obstacles (SiC particles in this case) is larger, the mean free path for crack propagation is shorter. Thereby the length of microcracks are shortened [45]. On the other hand, Kikuchi et al. [46] suggested that the presence of a hardened surface layer (Ti-Cu) on a ductile substrate (cp Ti) promoted microcrack initiation during tensile test due to the incompatibility of the brittle surface layer and the ductile substrate. When the cracks joined together, fracture, delamination and material loss occurred at the surface of the samples. In the present investigation, the hard IMPs of the laser-alloyed samples are resistant to electrical sliding wear as indicated by the less severe worn surface in Fig. 7(b). However, the high brittleness of the IMPs is very sensitive to the high load (50 N) for the electrical wear test and can lead to formation and propagation of cracks. The presence of the cracks at the surface further ascertains that delamination is possible during electrical sliding wear tests.

By XRD analysis, it was found that oxide peaks were only detected in LA-Ti-Cu-30 after sliding in dry condition, whereas no oxide peaks were detected in LA-Ti-Cu-20 after sliding in the same condition. Oxides detected on the worn surface of LA-Ti-Cu-30 in air confirmed that oxidative wear is also one of the wear mechanisms. The oxide will first act as a lubricant, but when the oxide breaks at a certain thickness, it will be detached as very small debris and result in mild material loss. During electrical sliding in dry condition, Cu-rich debris has been pulled out from LA-Ti-Cu-20 and adhered to the counterface steel disc. The protruding debris on the steel disc will cause cutting or ploughing on LA-Ti-Cu-20. The cutting process was so rapid that the growth of oxides may be hindered. LA-Ti-Cu-30 was rich in Ti-rich intermetallics. No metal transfer was found on the counterface steel disc and thus oxides were promoted under the high temperature during electrical sliding wear in dry conditions.

3.3.4 Worn debris

During the electrical sliding wear test, plate-like debris (approximately 1 mm x 1.5 mm) with high copper content has been pulled out from the sample LA-Cu-Ti-20. This phenomenon can be ascribed by the presence of ductile α -Cu in the alloyed layer. Cu has a rather low softening temperature (190 °C). It will be easily softened leading to rapid wear. As α -Cu was detected from the XRD spectra of the samples fabricated at 20 mm/s (Table 1), it can help to explain the slight increase in the wear rate for this sample. The worn debris was pulled out and its microstructure is shown in Fig. 8. EDX analyses shows that the debris mainly consist of: site A (3.6 wt.% Ti; 14.6 wt.% Cu; 42.0 wt.% Fe; O 39.8 wt.%); site B (10.6 wt.% Ti; 80.1 wt.% Cu; 3.0 wt.% Fe; O 6.4 wt.%); and site C (1.0 wt.% Ti; 95.2 wt.% Cu; 0.8 wt.% Fe; O 3.1 wt.%). The dark phase (site A) contains high Fe and O content. The brighter phases (sites B and C) are rich in Cu. No worn debris was obtained from the samples fabricated at high laser scanning speeds (25, 30 and 35 mm/s) after wear test because the debris was too small and few for collection. The samples fabricated at high scanning speeds possess more Ti-rich IMPs which are very hard to withstand wear. Moreover, no soft α -Cu was detected in LA-Ti-Cu-30 and LA-Ti-Cu-35 using XRD, showing minimal worn debris produced during electrical sliding wear.

4. Conclusions

- (1) Laser surface alloying of cp Cu with different Ti contents (25 to 85 wt.%) was achieved and their hardness was significantly enhanced. The highest hardness of the laser-alloyed sample fabricated at scanning speed of 30 mm/s (661 HV_{0.2}) is about 8.8 times that of cp Cu (75 HV_{0.2}).
- (2) The electrical sliding wear resistance of all laser-alloyed samples is significantly

increased by 3 orders of magnitude as compared with cp Cu. Among the laser-alloyed samples, the one fabricated at scanning speed of 30 mm/s possesses the highest electrical sliding wear resistance.

- (3) Wear rate increases with the presence of electric current and increase in sliding speed.
- (4) The enhancement in hardness and hence mechanical wear resistance of the laser-alloyed samples is attributed to solid solution strengthening and hard intermetallic phases.

Acknowledgements

The work described in this paper was fully supported by research grants from the Science and Technology Development Fund (FDCT) of Macau SAR (Grant Nos. 018/2008/A and 070/2011/A3, with the latter supporting X-ray diffraction experiments). The authors would also like to acknowledge Tescan China Ltd for their supports in preparation of TEM samples using FIB.

References

- [1] P.G. Slade, *Electrical contacts: principles and applications*, CRC, NY (1999) p. 403.
- [2] M. Braunovic and N.K. Myshkin, *Electrical contacts: fundamentals, applications and technology*, CRC Press, NY (2007) p. 71.
- [3] M. E.Abd El-Azim, H. M. Soliman, *J. Mater. Sci. Technol.* 13 (1997) 127-132.
- [4] K.T. Chiang, K.J. Kallenborn, J.L. Yuen, *Surf. Coat. Technol.* 52 (1992) 135-139.
- [5] A. Sanjurjo, B.J. Wood, K.H. Lau, G.T. Tong, D.K. Choi, M.C.H. McKubre, H. Song, *Surf. Coat. Technol.* 49 (1991) 103-109.
- [6] *ASM Handbook (Vol. 2): Properties and Selection: Nonferrous Alloys and*

- Special-Purpose Materials, ASM International, Materials Park, OH, 1990, 219; 529, 592.
- [7] T.J. Lonsbury, R.E. Fash, T.J. Russo, Proceedings of the Conference on Steelmaking, Bethlehem Steel Corp., (1992) 495-500.
- [8] U. Gelius, A.B. Kolpachev, O.V. Kolpacheva, I.Y. Nikiforov, A.A. Chularis, J. Struct. Chem. 42 (2001) 578-82.
- [9] C. Guo, J. Zhou, Y Yu, L Wang, H Zhou, J. Chen, Mater. Des. 36 (2012) 482-489.
- [10] W.R. Osorio, A. Cremasco, P.N. Andrade, A. Garcia, R. Caram, Electrochim. Acta 55 (2010) 759-770.
- [11] P. Franke, D. Neuschütz, Binary systems, Part 3: Binary Systems from Cs-K to Mg-Zr, Springer, Heidelberg, 2005, p.1-5.
- [12] T.B. Massalski, H. Okamoto, P.R. Subramanian, L. Kacprzak, Binary phase diagrams, 2nd Edition, ASM International, Materials Park, OH, 1990, p. 1495.
- [13] M. Reza Bateni, J.A. Szpunar, F. Ashrafizadeh, M. Zandrahimi, National Tribology Conference, (2003) 55-62.
- [14] V.A. Ravi, Pack Cementation Coatings, Corrosion: Fundamentals, Testing, and Protection, Vol 13A, ASM Handbook, ASM International, 2003, p 763–771.
- [15] C.Y. Liu, L.Y. Yu, W. Tian, J.C. Tang, Key Eng. Mater. 373-374 (2008) 354-357.
- [16] B.S. Xu, Key Eng. Mater. 373-374 (2008) 1-10.
- [17] X.D. Hu, Y. Zhang, J.H. Yao, Z.J. Chen, Adv. Mat. Res. 69-70 (2009) 338-342.
- [18] P.K. Wong, C.T. Kwok, H.C. Man, F.T. Cheng, Corros. Sci. 57 (2012) 228-240.
- [19] G. Dehm, B. Medres, L. Shepeleva, C. Scheu, M. Bamberger, B.L. Mordike, S. Mordike, G. Ryk, G. Halperin, I. Etsion, Wear 225-229 (1999) 18-26.
- [20] K.W. Ng, H.C. Man, F.T. Cheng, T.M. Yue, Appl. Surf. Sci. 253 (2007) 6236-6241.
- [21] M. Li, M. Chao, E. Liang, J. Yu, J. Zhang, D. Li, Appl. Surf. Sci. 258 (2011)

1599–1604.

- [22] P.K. Wong, C.T. Kwok, H.C. Man, Laser surface alloying of copper with titanium: Part II. Electrical wear resistance in wet and corrosive conditions, submitted to Surf. Coat. Technol.
- [23] J. Dutta Majumdar, I. Manna, Mater. Sci. Eng., A 268 (1999) 216–226.
- [24] J. Dutta Majumdar, I. Manna, Mater. Sci. Eng., A 268 (1999) 227–235.
- [25] J.M. Pelletier, A. Issa, P. Sallamand, Laser. Eng. 2 (1993) 81-92.
- [26] R. Jendrzewski, G. Sliwinski, Appl. Surf. Sci. 254 (2007) 921-925.
- [27] M. Franco, W. Sha, V. Tan, S. Malinov, Mater. Des. 85 (2015) 248-55.
- [28] R. Cao, Z. Feng, Q. Lin, J.H. Chen, Mater. Des. 56 (2014) 165-173.
- [29] D. Paulmier, A Bouchoucha, H. Zaidi, Vacuum 41 (1990) 2213-2216.
- [30] S.G. Jia, P. Liu, F.Z. Ren, B.H. Tian, M.S. Zheng, G.S. Zhou, Wear 262 (2007) 772-777.
- [31] B. Shanguan, Y.Z. Zhang, J.D. Xing, L.M. Sun, Y. Chen, Tribol. T. 53 (2010) 927-932.
- [32] A. Bouchoucha, S. Chekroud, D. Paulmier, Appl. Surf. Sci., 223, 330-342.
- [33] A. Bouchoucha, E.K. Kadiri, F. Robert, H. Zaidi, D. Paulmier, Surf. Coat. Technol. 76-77 (1995) 521-527.
- [34] A. Senouci, H. Zaidi, J. Frene, A. Bouchoucha, D. Paulmier, Appl. Surf. Sci. 144-145 (1999) 287-291.
- [35] M.R. Bateni, F. Asrafizadeh, J.A. Szpunar, R.A.L. Drew, Wear 253 (2002) 626-639.
- [36] D. Rigney, Fundamental of Friction and Wear of Materials, ASM International, Materials Park, OH, USA, 1981.
- [37] T.F.J. Quinn, Part VII of Fundamentals of Tribology, MIT Press, 1980, p. 477.
- [38] T. Sasada, S. Ban, S. Norose, T. Nakano, Wear 159 (1992) 191-199.

- [39] M.R. Bateni, S. Mirdamadi, F. Ashrafizadeh, J.A. Szpunar, R.A.L. Drew, Mater. Manuf. Processes 16 (2001) 219-228.
- [40] C. Ohkubo, I. Shimura, T. Aoki, S. Hanatani, T. Hosoi, M. Hattori, Y. Oda, T. Okabe, Biomaterials 24 (2003) 3377-2281.
- [41] S. Asadi Kouhanjani, A. ZareBidaki, A. Akbari, J. Alloy Compd. 486 (2009) 319-324.
- [42] S. Jacobson, S. Hogmark, Wear 266 (2009) 370-378.
- [43] F. Gao, H M. Wang, Intermetallics 16 (2008) 202-208.
- [44] M. Franco, W. Sha, G. Aldic, S. Malinov, H. Çimenoglu, Tribol. Int. 97 (2016) 265-71.
- [45] F. Masoumi, H.R. Ghasemi, A.A. Ziaei, D. Shahriari, Int. J. Adv. Manuf. Technol. 62 (2012) 1063–1070.
- [46] M. Kikuchi, Y. Takada, S. Kiyosue, M. Yoda, M. Woldu, Z. Cai, O. Okuno, T. Okabe, Dent. Mater. 19 (2003) 174-181.

Laser surface alloying of copper with titanium: Part II. Electrical wear resistance in wet and corrosive condition

C.T. Kwok^{a,b}, P.K. Wong^a, H.C. Man^c

^a Department of Electromechanical Engineering, University of Macau, China

^b Institute of Applied Physics and Materials Engineering, University of Macau, China

^c Department of Industrial and Systems Engineering, The Hong Kong Polytechnic University, Hong Kong, China

Abstract

Electrical sliding wear behavior of commercially pure copper (cp Cu) laser-alloyed with Ti in dry condition was reported in Part I of this paper. In Part II, the corrosion behavior in synthetic acid rain (SAR) and electrical sliding wear in distilled water (DW) and SAR of the laser-alloyed samples were investigated. Compared with cp Cu, corrosion resistance of the laser-alloyed samples in SAR was enhanced as evidenced by the reduction in corrosion current density, attributable to the presence of Ti for forming protective oxide. The electrical sliding wear resistance in DW and SAR was higher than that in dry environment because they acted as a lubricant and coolant for the sliding contact. For the samples tested in SAR, mechanical wear played the most important role, followed by corrosion-wear synergism, while corrosion was negligible. Measurements of interfacial contact resistance also showed that the electrical conductivity was inevitably compromised due to alloying with Ti in Cu.

Keywords: laser surface alloying; intermetallic phases; corrosion, wear, synergism, interfacial contact resistance

1. Introduction

Electrical contacts, which make and break electrical circuits, are used under different service conditions. Selection of an electrical contact material depends on a variety of factors including electrical and thermal conductivities, mechanical strength, wear and corrosion resistances and cost. However, no metallic material can possess all the desired properties for electric contact applications. Copper (Cu) is often used as contact material due to its excellent electrical and thermal conductivities and relatively low price as compared with silver and gold. Nevertheless, its low hardness and low softening temperature leads to electrical sliding wear. Moreover, the effect of environmental conditions also plays an important role in affecting the service lifespan of sliding couples [1-3]. For instance, copper contact wires and current collector of railway electrification systems operate in a variety of weather conditions such as dry, wet, acid rain, fog and even snow. Therefore, study on the electrical sliding wear of the contact materials in wet and corrosive conditions is necessary.

To improve the surface properties of Cu, laser surface alloying (LSA) of Cu with Ti has been attempted by using a high power diode laser (HPDL) [4]. Copper-titanium (Cu-Ti) intermetallic compounds are reported to have high hardness and are good electric conductors [6-8]. In the corrosion studies of Cu-Ti alloys in 0.9 wt.% NaCl solution [9, 10], addition of 5 - 30 wt.% of Cu to Ti was found to increase the corrosion rate as compared with pure Ti [9]. While the passive current densities of Ti alloyed with 5 - 20 wt.% Cu and pure Ti in 0.9 wt.% NaCl solution below 1.4 V were the same, and current density increases with Cu content as the potential reached the transpassive region [10]. Precipitation of CuTi_2 in the Cu-Ti alloys slightly increased the corrosion current density but the passive film did not appear to break down with the presence of such intermetallic. On the other hand, corrosion properties of

laser-alloyed Cu-Ti layers with 25 to 85 wt.% Ti in 3.5 wt.% NaCl solution at 25 °C have been reported in a previous study of the present authors [4]. The corrosion potentials of the laser-alloyed samples are found to be actively shifted with the increase in Ti content but their corrosion current densities are lower than that of cp Cu. The laser-alloyed Cu-Ti coating fabricated at scanning speed of 35 mm/s has corrosion resistance 150 times that of cp Cu, being very close to that of cp Ti [4].

In Part I of this paper, the microstructure, compositions, phase present and electrical sliding wear behavior of the laser-alloyed samples in dry condition have been reported [5]. However, sliding electrical contacts are often used in outdoor environments, and literatures related to electrical sliding wear behavior of laser-alloyed Cu-Ti samples in wet and corrosive conditions is extremely scarce. Electrical sliding wear behavior with corrosive medium should not be overlooked since acid rain is a natural electrolyte which may cause adverse corrosive effects on electric contact materials used in outdoor environments. In Part II, the corrosion behavior and electrical sliding wear behavior of the laser-alloyed Cu-Ti layers in SAR are evaluated. Moreover, the relative contributions of mechanical wear, electrochemical corrosion and corrosion-wear synergism to the overall wear damage are elucidated.

2. Experimental details

Fabrication of laser-alloyed cp Cu with Ti samples with different laser processing conditions has been described in Part I of this paper. To investigate the electrochemical behavior of the laser-alloyed samples, cp Cu and cp Ti in stagnant SAR solution (open to air) at 25 ± 1 °C, open-circuit potential (*OCP*) measurement and potentiodynamic polarization test were conducted using a potentiostat (PAR Versastat II) in accordance with ASTM standard G5-92 [11]. All potentials were measured with

respect to the reference saturated calomel electrode (SCE, 0.244V versus SHE at 25 °C). Two parallel graphite rods were applied as the counter electrode for current measurement. The final steady *OCP* value was recorded after a measurement of 120 minutes and the potential was then increased at a rate of 1 mV/s; starting from 0.2 V_{SCE} below the *OCP*. Corrosion current density (I_{corr}) was extracted by Tafel extrapolation with the aid of commercial software (PowerCorr, V.2.42) after the potentiodynamic polarization tests.

Electrical sliding wear testing in dry condition was conducted using a pin-on-disc tribometer as described in Part I [5]. The wear tests in wet conditions were conducted at a constant load of 50 N, sliding speed of 40 km/h and 60 km/h, with and without DC current (60 A) in SAR (pH 3.5) and distilled water (DW) (pH 7). SAR or DW was dropped to the laser-alloyed surface with a constant flow rate of 30 mL/min with a flowmeter. As a matter of fact, there is no standard composition/preparation of the SAR. The SAR was prepared according to the rain composition obtained by The Macao Meteorological and Geophysical Bureau (SMG) in 2012 [12]. The content will not vary too much as compared with other literature [13, 14]. In general, the rainwater contains mainly sulphate, nitrate, chloride and hydrogen ions. The composition of the SAR used in the present study is: SO_4^{2-} 31 mg/L, NO_3^- 11 mg/L, Cl^- 27.3 mg/L, Na^+ 27.3 mg/L, Ca^{2+} 5.5 mg/L with a measured pH of 3.5. Due to the presence of electric current and water, electric arc was produced leading to arc erosion.

The weight loss ΔW (in g) of the samples was intermittently recorded at a time interval of 1 minute (for sliding at 60 km/h) or 1.5 minute (for sliding at 40 km/h) and the average wear (thickness) loss (Δd) was calculated by:

$$\Delta d \text{ (mm)} = 10 \frac{\Delta W}{\rho A} \quad (1)$$

where ρ (in g/cm^3) and A (in cm^2) are the density and the exposed surface area of cp Cu or the laser-alloyed layers respectively according to Part I [5]. The average rates of

wear loss of materials are expressed in terms of the wear rate in DW without electrochemical corrosion (E) and wear-corrosion rate in SAR (T). The wear rate in dry condition (D) was obtained in Part I. Synergistic effect between electrical wear and corrosion of the laser-alloyed specimens in SAR was analyzed. To investigate the synergism between electrical wear and corrosion, wear-corrosion synergism S is calculated according ASTM standard G119-04 using equation (2) [13, 15, 16]. For the sake of convenient comparison with the results of others, the decomposition by loss mechanism was defined in the ASTM standard.

$$S = T - E - C \quad (2)$$

where C is the corrosion rate of the samples in SAR calculated from the I_{corr} (Table 1) according to ASTM standard G102-89 [17]:

$$C \text{ (mm yr}^{-1}\text{)} = K \left(\frac{I_{corr}}{\rho} \right) EW \quad (3)$$

where K is a constant = $3.27 \times 10^{-3} \text{ mm g } \mu\text{A}^{-1} \text{ cm}^{-1} \text{ yr}^{-1}$, I_{corr} is the corrosion current density in $\mu\text{A cm}^{-2}$, ρ is the density obtained from equation (3) in g cm^{-3} in Part I, and EW is the equivalent weight, which is defined as follows:

$$EW = \left(\sum \frac{n_i W_i}{A_i} \right)^{-1} \quad (3)$$

where W_i is the weight fraction, n_i is the valence, and A_i is the atomic mass of the i^{th} element in the sample.

After electrical sliding wear tests, the worn surface from the samples were analysed using a scanning-electron microscope (SEM, Hitachi S-3400N) equipped with an energy dispersive X-ray spectrometer (EDX, Horiba EX-250), while phase constitution was identified using X-ray diffractometry (XRD, Rigaku MiniFlex 600) with $\text{CuK}\alpha$ radiation operating at 40 kV and 15 mA at a scan rate of 0.1 °/s.

Fig. 1 shows the schematic diagram of the setup for interfacial contact resistance (ICR) measurement which has been previously described [18]. The laser-alloyed

sample was machined to a square plate with surface area of 10 mm × 10 mm. Compression force of 15 to 115 N/cm² was applied by a motorized force tester (LTCM-500, Chatillon) and the resistance was measured by connecting two Cu plates with a DC ohmmeter with an accuracy of ±1 μΩ (GOM-802, Gwinstek). The total measured resistance is a sum of two interfacial components. For cp Cu without the laser-alloyed layer, the two interfacial components are the same, which is two cp Cu (substrate) /Cu plate interfaces ($2R_{Cu/Cu}$), whereas for the laser-alloyed specimen, the interfacial components consisted of a cp Cu (substrate)/Cu plate ($R_{Cu/Cu}$) and a laser-alloyed layer/Cu plate interface (R_c). The calculation of ICR of the laser-alloyed layer/Cu plate interface is shown in equation (4).

$$R_c = R_m - R_{Cu/Cu} \quad (4)$$

where $R_c = ICR$ of the laser-fabricated layer/Cu plate interface; $R_m =$ measured resistance by the ohmmeter; $R_{Cu/Cu} = ICR$ of Cu substrate /Cu plate interface, which is a constant at a certain compression force.

3. Results and discussion

3.1 Corrosion behavior in SAR

The plot of OCP vs time and the potentiodynamic polarization curves for the laser-alloyed samples, cp Cu and cp Ti in SAR solution (pH 3.5, open to air) at 25 °C are shown in Fig. 2. The extracted OCP values and corrosion current densities (I_{corr}) are summarized in Table 1.

Generally, the corrosion behavior of alloys containing IMPs depends on the relative volume fraction, compositional distribution and reactivity of the IMPs and metallic phases, which might lead to microgalvanic coupling [19-22]. The existence of the IMPs in the alloy matrix can be either noble (cathodic) or active (anodic). Based on the Pourbaix diagrams and the OCP for Cu and Ti, Cu is cathodic while Ti

is anodic but self-passivating in SAR. As a result, neither α -Cu nor α -Ti corrodes spontaneously. The IMPs in the laser-alloyed samples are then probably the sacrificial anodes according to the fact that the OCP and I_{corr} values of the laser-alloyed samples are lower than cp Cu but higher than cp Ti (Fig. 2 and Table 1). The ranking of OCP of the various samples in SAR is:

$$\text{cp Ti} > \text{LA-Ti-Cu-35} \sim \text{LA-Ti-Cu-30} \sim \text{LA-Ti-Cu-25} > \text{LA-Ti-Cu-20} > \text{cp Cu}$$

Based on the I_{corr} , the ranking of corrosion resistance in SAR of the specimens is:

$$\text{cp Ti} > \text{LA-Ti-Cu-35} > \text{LA-Ti-Cu-30} > \text{LA-Ti-Cu-25} > \text{LA-Ti-Cu-20} > \text{cp Cu}$$

The above ranking is consistent with that of samples tested in 3.5 wt.% NaCl solution [4]. The I_{corr} of LA-Ti-Cu-20 was the highest among all laser-alloyed specimens. The I_{corr} of LA-Ti-Cu-35 was close to cp Ti and was about 38 times lower than that of cp Cu.

For the laser-alloyed samples fabricated at a scanning speed of 20 mm/s, α -Cu was the major phase in addition to the minor phases of Cu-rich IMP (Cu_4Ti). The Cu-rich IMPs are more active (anodic) than α -Cu (cathodic) as evidenced by the variation of E_{corr} for LA-Ti-Cu-20 with time, going from above cp Cu and to below cp Cu finally (Fig. 2a). The small anodic area ratio of IMPs coupled with large cathodic α -Cu is expected to have the highest corrosion rate among all the laser-alloyed specimens [4]. Although LA-Ti-Cu-25 specimens also possess α -Cu in the alloyed layer, the major phases present were IMPs. The large anodic area ratio of IMPs to small cathodic area ratio of α -Cu has a less pronounced effect on corrosion rate [4]. The ability of forming a passive oxide layer also contributes to the increase in corrosion resistance when compared to LA-Ti-Cu-20. For the samples fabricated at higher scanning speeds (30 – 35 mm/s), the major phases present are Ti-rich IMPs with addition to minor phase of α -Ti. Although α -Ti is more active than the IMPs which resulted in a small area ratio of anode to cathode, the stable passive oxide layer

formed on these specimens can significantly protect the coatings from corrosion attack. Fig. 3 shows the SEM micrographs of the laser-alloyed samples after potentiodynamic polarization tests in SAR. It can be observed that the corrosion attack for the sample with lower Ti content (LA-Ti-Cu-20) is more serious while the sample with higher Ti content (LA-Ti-Cu-30) reveals a milder corrosion attack due to the presence of passive Ti oxide layer. Copper was oxidized as the corrosion products, whereas a protective Ti oxide layer was formed for samples with high Ti content to resist corrosion attack. The effect of addition Ti to Cu is similar to alloying Cu with Cr, in which the CuCr47 alloy is reported to form a passive film on the surface and the corrosion resistance of pure copper is obviously enhanced [23-25].

3.2 Electrical sliding wear behavior in wet conditions

The cumulative thickness loss against distance traveled of various laser-alloyed samples worn at 60 km/h with and without a DC current in wet conditions (DW and SAR) are typically shown in Fig. 4 (while the data obtained at 40 km/h is shown in Table 2). The plot of wear rates of various samples is depicted in Fig. 5 and the values of wear rate are given in Table 2. Similar to the results of electrical sliding wear in dry conditions as discussed in Part I [5], the wear rates of all laser-alloyed samples in wet conditions are much lower than that of cp Cu due to the hard IMPs and solid solution strengthening. The wear performance of alloys depends on the operating conditions such as sliding speed, contact force, current intensity, level of arcing and environmental factors [26, 27]. Wear rates increase with increase in sliding speed and application of electric current as shown in Table 2. Although the presence of electric current and water will enhance the occurrence of electric arc, the wear rates of laser-alloyed samples and cp Cu in wet condition are smaller than those in dry condition (i.e. $D > T > E$) due to the lubricating and cooling effect of DW or SAR [28].

The worn surface of the laser-alloyed samples after sliding in dry condition looks to be a blue tint whereas the worn surface after sliding in wet condition remains silvery in color. Such observations confirm that wet wear reduced the wear rate because DW and SAR acted as a lubricant and coolant for lubricating and decreasing the temperature of the sliding contacts. The degree of surface damage of the cp Cu after electrical sliding wear test in wet environment was not as severe as in dry wear (Fig. 6). Although some adhesive patches were found on the counterface steel disc after electrical sliding wear test in wet conditions, the wear rates of cp Cu obtained in wet conditions were still much higher than those of the laser-alloyed specimens. Adhesive and abrasive wear were the dominating wear mechanism in wet sliding environments. From the infrared temperature sensor measurement, the temperature of the laser-alloyed samples and cp Cu sliding in wet conditions was about 28 °C only. This elucidated that softening temperature of cp Cu has not been reached and the wear rate can be reduced in wet sliding environment. No worn debris has been obtained from all laser-alloyed samples.

Electrical sliding wear resistance of the laser-alloyed samples in DW and SAR tends to increase with the increase in surface hardness. Consistently, LA-Ti-Cu-30 possesses the highest electrical wear resistance in wet conditions among all laser-alloyed samples as in the dry wear condition. This supported that the presence of the hard IMPs and solid solution strengthening enhances the wear resistance in both wet and dry conditions. Besides, the hardness of the worn surface of the laser-alloyed samples after wet electrical sliding wear test is markedly harder than that before wear tests as shown in Table 3. Dislocation strengthening (work hardening) due to the plastic deformation also plays a role in improving the electrical wear resistance. The ranking of electrical wear resistance in DW and SAR of various laser-alloyed specimens at 60 km/h and 60 A is:

LA-Ti-Cu-30 > LA-Ti-Cu-35 ~ LA-Ti-Cu-25 > LA-Ti-Cu-20 >> cp Cu

and consistent with that in dry condition. From Table 2, the ranking of wear and corrosion rates and synergism are as follows:

$$D > T > E > S >> C$$

C is much smaller than the wear rates (*D*, *T* and *E*) while *S* shows some contribution to *T*.

For the laser-alloyed samples with low Ti content (LA-Ti-Cu-25 and LA-Ti-Cu-20) and cp Cu worn in SAR, the samples were corroded and a surface film was produced, with simultaneous occurrence of sliding wear. The sample surface was corroded and soluble corrosion products (e.g. sulphate and chloride) were formed in SAR (Fig. 3a). For the laser-alloyed samples with higher Ti content (LA-Ti-Cu-30 and LA-Ti-Cu-35) that were worn in SAR, the samples were passivated when insoluble corrosion product films were formed in SAR due to the existence of more Ti (Fig. 3b). Their corrosion product films consist of brittle oxides / hydrated oxide but are easily removed during sliding wear. For both cases, the samples have a short lifetime under electrical sliding wear and a higher wear rate may occur due to repeated destruction and regrowth of the films [29].

After electrical sliding wear test in SAR, the thickness of LA-Ti-Cu-30 was reduced from 0.4 mm to 0.22 mm. On other hand, the thickness of LA-Ti-Cu-20 was reduced from 0.8 mm to 0.4 mm. The worn surface and cross sectional view of LA-Ti-Cu-30 and LA-Ti-Cu-20 are typically shown in Fig. 6. Despite the enhancement in wear resistance of the laser-alloyed samples, the presence of cracks reflected that large amount of material loss will arise when the cracks propagate and join together. For LA-Ti-Cu-20 with high content of ductile α -Cu phase and smaller amount of hard IMPs, no crack was observed. For LA-Ti-Cu-30 with high content of hard IMPs, the alloyed layer is prone to cracking [Fig. 6(b)(ii)]. The combination of

the hard IMPs together with ductile α -Cu phase can enhance the wear behavior of the laser-alloyed samples. Hard phases can reduce the amount of transferred load to the Cu binder. The cracking in samples with high content of IMPs suggested that ductility is also an important concern in addition to hardness. Thus, the sample fabricated at a scanning speed of 20 mm/s (LA-Ti-Cu-20) could enhance the hardness by 4.8 times when compared to cp Cu while the ductility of the alloyed layer was maintained and was not susceptible to cracking.

3.3 Synergistic effect

From the contributions of mechanical and arcing, corrosion and synergistic effects of the samples after electrical sliding wear in DW and SAR at 40 and 60 km/h with and without current as shown in Table 2, it can be observed that the samples sliding in the presence of SAR possess a higher wear rate than in DW ($T > E$), indicating that corrosion accelerates the wear rates. SAR has a lower pH and contains sulphate, nitrate, chloride ions which are more corrosive than DW. Cu is susceptible to sulphate and chloride ions attack and a local breakdown of the oxide layer will initiate corrosion attack owing to preferable adsorption of the chloride ions and thus hindering repassivation at local sites [13, 30, 31]. Ragab et al reported that the corrosive wear resistance of bronze composites decreases as the pH values of the wet media decrease [14]. The wear rates of the samples in SAR are slightly higher than those in DW. In general when sliding in wet conditions, the dominating mechanism is ascribed to the mechanical and arcing effect, as shown by high contributions from E/T . When sliding in SAR solution, wear loss is dominated by delamination of the hard and brittle alloyed layer, detachment of worn debris and corrosion products. The removal of corrosion products during electrical sliding wear would lead to the exposure of a fresh surface to the SAR, which would form more corrosion products.

The synergistic effect (S/T) for the laser-alloyed samples could reach about 20.2%, reflecting that synergism of wear and corrosion also contributes to wear damage during electrical sliding wear in SAR while corrosion alone is negligible.

3.4 Interfacial contact resistance

The plot of ICR of cp Cu and the laser-alloyed samples versus applied compressive force is shown in Fig. 7. The steady values of the ICR at 50 N/cm² are listed in Table 3. With the addition of Ti (420 n Ω ·m) which has a much higher resistivity when compared to Cu (17 n Ω ·m), the ICR values of all the laser-alloyed samples have increased to 0.158 – 1.134 m Ω ·cm² (about 5 - 37 times that of cp Cu) as the Ti content increases from 25 to 85 wt%. It was reported that an 80 μ m sandwich layer of Mo–Ni–Cu on copper fabricated by laser cladding had a specific contact resistance of about 56.3 $\mu\Omega$ ·cm² (the resistivity of Mo and Ni are 53 and 70 n Ω ·m, respectively) [32]. Compared with the laser-cladded Cu with Mo–Ni, the ICR of the laser-alloyed Cu with Ti is higher, probably attributable to the higher resistivity of Ti and the much thicker alloyed Cu–Ti layers (350 – 800 μ m). On the other hand, in the study of addition of 2.5 wt.% TiB₂ to Cu for increasing wear resistance, the electrical resistivity was increased by 8 times [33]. The ceramic phase TiB₂ in Cu–TiB₂ composites and similarly the intermetallic phases in the laser-alloyed Cu–Ti acted as scattering centers and the electricity resistivity increased with the concentration of Ti or TiB₂ in the alloys or composites [32, 33].

Thus, it is not surprising that the ICR values increase with the amount of Ti content in the alloyed layers. Among all laser-alloyed samples, LA–Ti–Cu–20 has the lowest ICR values and is closest to the value for cp Cu. On the other hand, LA–Ti–Cu–35 has the highest ICR value. The ranking of the ICR is:

$$LA-Ti-Cu-35 > LA-Ti-Cu-30 > LA-Ti-Cu-25 > LA-Ti-Cu-20 > cp Cu$$

Although the addition of Ti to Cu will increase resistivity, corrosion and wear resistances of the alloyed layers will be enhanced. In fact, no material can possess all the desired properties for all electric contact applications. Thus it is important to get a balance of the properties that has the best overall performance during actual application. In the present study, the laser-alloyed samples fabricated at scanning speeds of 25, 30 and 35 mm/s possess CuTi_2 as their major phase in the alloyed layers. Although these samples possess a higher hardness to resist wear as well as a higher corrosion resistance due to the presence of a protective oxide film, the brittleness of the hard IMPs results in cracks during electrical sliding wear. When the cracks join together, large amount of material loss will consequently arise. Thus, the sample LA-Ti-Cu-20 which possesses *ICR* values close to that of cp Cu and electrical sliding wear and corrosion resistance higher than cp Cu is concluded to have the best overall performance among all the laser-alloyed samples.

4. Conclusions

- (1) Laser surface alloying of cp Cu with different Ti contents (25 to 85 wt.%) were achieved by high power diode laser.
- (2) The corrosion current densities of all laser-alloyed samples in synthetic acid rain are lower than that of cp Cu. LSA of cp Cu with Ti fabricated at scanning speed of 35 mm/s showed the highest corrosion resistance, that is, about 38 times that of cp Cu and very close to that of cp Ti. The corrosion resistance ranking is:
 $\text{cp Ti} > \text{LA-Ti-Cu-35} > \text{LA-Ti-Cu-30} > \text{LA-Ti-Cu-25} > \text{LA-Ti-Cu-20} > \text{cp Cu}$.
- (3) The enhancement in corrosion resistance of the laser-alloyed samples in SAR is attributed to the presence of Ti in the intermetallic and metallic phases for forming the partial protective oxide.
- (4) The wear rates in wet conditions increase with sliding speed and electrical

current, similar to the dry condition. Generally, the wear rates of the specimens in different conditions are as follows:

$$D > T > E > S \gg C$$

- (5) The main contribution of electrical sliding wear in SAR is mechanical wear, with contribution of corrosion-wear synergism up to 20.2%, while corrosion alone is negligible.
- (6) Interfacial contact resistance of the laser-alloyed layers is compromised. The *ICR* values of the laser-alloyed samples increase with the amount of Ti present in the alloyed layers.
- (7) Among all laser-alloyed samples, LA-Ti-Cu-20 with the lowest *ICR* value and absence of cracking after electrical wear, has the best overall performance.

Acknowledgements

The work described in this paper was fully supported by research grants from the Science and Technology Development Fund (FDCT) of Macau SAR (Grant Nos. 018/2008/A and 070/2011/A3, with the latter supporting X-ray diffraction experiments).

References

- [1] C.R.F. Azevedo, A. Sinatora, *Eng. Fail. Anal.* 11 (2004) 829-841.
- [2] Y. Oura, Y. Mochinaga, H. Nagasawam, *JRTR* 16 (1998) 48-58.
- [3] A. Senouci, H. Zaidi, J. Frene, A. Bouchoucha, D. Paulmier, *Appl. Surf. Sci.* 144-145 (1999) 287-291.
- [4] P.K. Wong, C.T. Kwok, H.C. Man, F.T. Cheng, *Corros. Sci.* 57 (2012) 228-240.
- [5] P.K. Wong, C.T. Kwok, H.C. Man, Laser surface alloying of copper with titanium: Part I. Electrical wear resistance in dry conditions, submitted to *Surf.*

Coat. Technol.

- [6] U. Gelius, A.B. Kolpachev, O.V. Kolpacheva, I.Y. Nikiforov, A.A. Chularis, J. Struct. Chem. 42 (2001) 578-82.
- [7] C. Guo, J.S. Zhou, Y.J. Yu, L.Q. Wang, H.D. Zhou, J. M. Chen, Mater. Des. 36 (2012) 482-489.
- [8] W.R. Osorio, A. Cremasco, P.N. Andrade, A. Garcia, R. Caram, Electrochim. Acta 55 (2010) 759-770.
- [9] Y. Takada, H. Nakajima, O. Okuno, T. Okabe, Dent. Mater. J. 20 (2001) 34-52.
- [10] Y. Takada, O. Okuno, Dent. Mater. J. 24 (2005) 610-615.
- [11] ASTM standard G5-92: Standard Reference Test Method for Making Potentiodynamic Anodic Polarization Measurement, ASTM Standards, Philadelphia (1994).
- [12] Macao Meterological and Geophysical Bureau, Annual report of air quality, Macao Meterological and Geophysical Bureau, (2012), p. 1-66
http://www.smg.gov.mo/www/ccaa/report/pdf/IQA_Y/IQA_2012.pdf
- [13] H. Ding, G. Zhou, Z. Dai, Y. Bu, T. Jiang, Wear (2009) 292-298
- [14] Kh. A. Ragab, R. Abdel-Karim, S. Farag, S. M. EI-Raghy, H. A. Ahmed, Tribol. Int. (2010) 594-601.
- [15] ASTM standard G119-04: Standard Guide for Determining Synergism between Wear and Corrosion Annual Book of ASTM Standards, Vol. 03.02. Philadelphia (2004).
- [16] C.T. Kwok, F.T. Cheng, H.C. Man, Surf. Coat. Technol. 145 (2001) 206-214.
- [17] ASTM standard G102-89: standard Practice for Calculation of Corrosion Rates and Related Information from Electrochemical Measurements, Annual Book of ASTM Standards, Vol. 03.02. Philadelphia (1989).
- [18] H.L. Wang, M.A. Sweikart, J.A. Turner, J. of Power Sources 115 (2003) 243.

- [19] R. Ambat, N.N. Aung, W. Zhou, *Corros. Sci.* 42 (2000) 1433-1455.
- [20] N.N. Aung, W. Zhou, *J. Appl. Electrochem.* 32 (2002) 1397-1401.
- [21] W. Zhou, N.N. Aung, Y.S. Sun, *Corros. Sci.* 51 (2009) 403-408.
- [22] N.N. Aung, W. Zhou, *Corros. Sci.* 52 (2010) 589-594.
- [23] G.Y. Fu, Y. Niu, W.T. Wu, *Nonferrous Met. Soc. China* 11 (2001) 532-536.
- [24] J.H. Liu, Y.M. Gao, X.Q. Zhang, *Shanghai Nonferrous Metals* 24 (2003) 149-157.
- [25] Y.N. Zhang, J.L. Zi, M.S. Zheng, J.W. Zhu, *J. Alloys Compd.* 462 (2008) 240-243.
- [26] F. Kießling, R. Puschmann, A. Schmieder, *Contact Lines for Electric Railways: Planning, Design and Implementation*, Publics Cooperate Publishing, Munich Erlangen (2001) p. 83.
- [27] B. Pizzigoni, A. Collina, B. Flapp, S. Melzi, *Tribotest* 13 (2007) 35-47.
- [28] Y. Wang, L. Zhang, J. Xiao, W. Chen, C. Feng, X. Gan, K. Zhou, *Tribol. Int.* 94 (2016) 260-268.
- [29] G.W. Stachowiak, A.W. Batchelor, Chapter 13: Corrosion and oxidative wear, *Engineering Tribology*, 4th Edn, Elsevier Incorporation (2014) p. 598.
- [30] K.P. Fitzgerald, J. Nairn, A. Atrens, *Corros. Sci.* 40 (1998) 2029-2050.
- [31] G. Kear, B.D. Barker, F.C. Walsh, *Corros. Sci.* 46 (2004) 109-135.
- [32] K.W. Ng, H.C. Man, F.T. Cheng, T.M. Yue, *Appl. Surf. Sci.* 253 (2007) 6236-6241.
- [33] J.P. Tu, W. Rong, S.Y. Guo, Y.Z. Yang, *Wear* 255 (2003) 832-835.

Part I

Legend of Tables

Table 1. Laser parameters, compositions, phase present, and coating thickness of laser-alloyed samples, cp Cu and cp Ti.

Table 2. Hardness and susceptibility to cracking for various samples.

Table 3. Wear rates values of cp Cu and laser-alloyed samples tested in various speeds, and current intensities in dry condition.

Part I

Sample	Scanning speed (mm/s)	Thickness of alloyed layer D (mm)	Dilution ratio DR (%)	Average Ti content (%)	Major phase	Minor phase(s)
cp Cu	-	-	-	0	α -Cu	–
LA-Ti-Cu-20	20	0.80	62.5	25	α -Cu	Cu ₄ Ti
LA-Ti-Cu-25	25	0.45	33.3	50	CuTi ₂	Cu ₄ Ti ₃ , CuTi, Cu ₄ Ti, α -Cu, CuO
LA-Ti-Cu-30	30	0.40	25.0	70	CuTi ₂	Cu ₄ Ti ₃ , CuTi, Cu ₄ Ti, α -Ti
LA-Ti-Cu-35	35	0.35	14.3	85	CuTi ₂	Cu ₄ Ti ₃ , CuTi, α -Ti
cp Ti	-	-	-	100	α -Ti	–

Table 1. Laser parameters, compositions, phase present, and coating thickness of laser-alloyed samples, cp Cu and cp Ti.

Sample	Average hardness (HV _{0.2})	Average hardness after worn in air 60 km/ 60A (HV _{0.2})	Susceptibility to cracking in air
cp Cu	75 ± 2	95 ± 5	No
LA-Ti-Cu-20	362 ± 17	458 ± 157	No
LA-Ti-Cu-25	568 ± 51	639 ± 219	Yes
LA-Ti-Cu-30	661 ± 41	790 ± 96	Yes
LA-Ti-Cu-35	541 ± 29	752 ± 127	Yes

Table 2. Hardness and susceptibility to cracking for various samples.

Wear condition	Sample	Wear rate in dry condition D (mm/h)
40 km/h, 0 A	LA-Ti-Cu-20	0.84
	LA-Ti-Cu-25	0.65
	LA-Ti-Cu-30	0.54
	LA-Ti-Cu-35	0.47
	cp Cu	166
40 km/h, 60 A	LA-Ti-Cu-20	0.78
	LA-Ti-Cu-25	0.80
	LA-Ti-Cu-30	0.69
	LA-Ti-Cu-35	0.62
	cp Cu	192
60 km/h, 0 A	LA-Ti-Cu-20	1.38
	LA-Ti-Cu-25	1.12
	LA-Ti-Cu-30	0.99
	LA-Ti-Cu-35	1.00
	cp Cu	279
60 km/h, 60 A	LA-Ti-Cu-20	1.56
	LA-Ti-Cu-25	1.32
	LA-Ti-Cu-30	1.03
	LA-Ti-Cu-35	1.24
	cp Cu	293

Table 3. Wear rate values of cp Cu and laser-alloyed samples tested in various speeds, and current intensities in dry condition.

Part II

Legend of Tables

Table 1. Open circuit potentials (*OCP* vs *SCE*) and corrosion current densities (I_{corr}) of various laser-alloyed samples, cp Cu and cp Ti in SAR solution (open to air) at 25 °C.

Table 2. Wear rate values of cp Cu and laser-alloyed samples tested in various speeds, current intensities and environments.

Table 3. Hardness, susceptibility to cracking and *ICR* for various samples.

Part II

Sample	<i>OCP vs SCE</i> (V_{SCE})	I_{corr} ($\mu A/cm^2$)
cp Cu	-0.055	1.570
LA-Ti-Cu-20	-0.082	0.697
LA-Ti-Cu-25	-0.155	0.406
LA-Ti-Cu-30	-0.160	0.075
LA-Ti-Cu-35	-0.136	0.041
cp Ti	-0.232	0.018

Table 1. Open circuit potentials (*OCP vs SCE*) and corrosion current densities (I_{corr}) of various laser-alloyed samples, cp Cu and cp Ti in SAR solution (open to air) at 25 °C.

Wear condition	Sample	Wear/corrosion rate (mm/h)					<i>E/T</i> %	<i>S/T</i> %	<i>C/T</i> % 10 ⁻⁶
		<i>D</i> (in air)	<i>E</i> (in DW)	<i>T</i> (in SAR)	<i>C</i> (in SAR) 10 ⁻⁶	<i>S</i>			
40 km/h, 0 A	LA-Ti-Cu-20	0.84	0.53	0.56	1.63	0.03	94.6	5.4	291
	LA-Ti-Cu-25	0.65	0.57	0.58	0.89	0.01	98.3	1.7	153
	LA-Ti-Cu-30	0.54	0.38	0.41	0.16	0.03	92.7	7.3	39.0
	LA-Ti-Cu-35	0.47	0.35	0.42	0.08	0.07	83.3	16.7	19.0
	cp Cu	166	130	151	4.16	21.6	85.7	14.3	2.76
40 km/h, 60 A	LA-Ti-Cu-20	0.78	0.56	0.68	1.63	0.12	82.4	17.6	240
	LA-Ti-Cu-25	0.80	0.53	0.58	0.89	0.05	91.4	8.6	153
	LA-Ti-Cu-30	0.69	0.58	0.62	0.16	0.04	93.5	6.5	25.8
	LA-Ti-Cu-35	0.62	0.52	0.56	0.08	0.04	92.9	7.1	14.3
	cp Cu	192	177	186	4.16	8.75	95.3	4.7	2.24
60 km/h, 0 A	LA-Ti-Cu-20	1.38	0.76	0.88	1.63	0.12	86.4	13.6	185
	LA-Ti-Cu-25	1.12	0.73	0.78	0.89	0.05	93.6	6.4	114
	LA-Ti-Cu-30	0.99	0.58	0.62	0.16	0.04	93.5	6.5	25.8
	LA-Ti-Cu-35	1.00	0.65	0.68	0.08	0.03	95.6	4.4	11.8
	cp Cu	279	214	221	4.16	7.32	96.7	3.3	1.89
60 km/h, 60 A	LA-Ti-Cu-20	1.56	1.13	1.18	1.63	0.05	95.8	4.2	138
	LA-Ti-Cu-25	1.32	0.92	1.05	0.89	0.13	87.6	12.4	84.8
	LA-Ti-Cu-30	1.03	0.79	0.99	0.16	0.20	79.8	20.2	16.2
	LA-Ti-Cu-35	1.24	0.90	1.05	0.08	0.15	85.7	14.3	7.61
	cp Cu	293	223	270	4.16	46.8	82.6	17.4	1.55

Table 2. Wear rate values of cp Cu and laser-alloyed samples tested in various speeds, current intensities and environments.

Sample	Average hardness (HV _{0.2})	Average hardness after worn in SAR 60 km/ 60A (HV _{0.2})	Susceptibility to cracking in SAR	ICR at 50 N/cm ² (mΩ·cm ²)
cp Cu	75 ± 2	97 ± 5	No	0.031
LA-Ti-Cu-20	362 ± 17	457 ± 108	No	0.158
LA-Ti-Cu-25	568 ± 51	671 ± 256	Yes	0.808
LA-Ti-Cu-30	661 ± 41	681 ± 156	Yes	0.926
LA-Ti-Cu-35	541 ± 29	727 ± 111	Yes	1.134

Table 3. Hardness, susceptibility to cracking and *ICR* for various samples.

Part I

Legends of figures

Fig. 1. Schematic diagram of pin-on-disc tribometer: (A) rotating disc; (B) high speed motor; (C) bearing support; (D) specimen; (E) specimen holder; (F) power supply; (G) force sensor; (H) manometer; (I) oil control valves; (J) oil pressure pump and tank.

Fig. 2. Laser-alloyed specimen fabricated at scanning speed of 30 mm/s (LA-Ti-Cu-30) showing: (a) cross-sectional view, (b) microstructures and (c) interface between the alloyed layer and substrate.

Fig. 3. XRD patterns of laser-alloyed specimens fabricated at scanning speeds of (a) 20 mm/s, (b) 25 mm/s, (c) 30 mm/s and (d) 35 mm/s.

Fig. 4. Hardness profiles of various laser-alloyed samples.

Fig. 5. (a) Cumulative thickness loss against distance traveled for various specimens in dry wear at (i) 60 km/h, 0 A, (ii) 60 km/h, 60 A and (b) electrical wear rates of various laser-alloyed samples and cp Cu.

Fig. 6. TEM micrographs of LA-Ti-Cu-30 (a) before and (b) after electrical sliding wear at 60 km/h and 60 A, in dry condition.

Fig. 7. Worn morphology of (a) LA-Ti-Cu-20 and (b) LA-Ti-Cu-30 at 60 km/h, 60A in SAR (i) surface view and (ii) cross-sectional view.

Fig. 8. Debris pulled out from LA-Ti-Cu-20 sliding at 60 km/h, 60 A in dry condition.

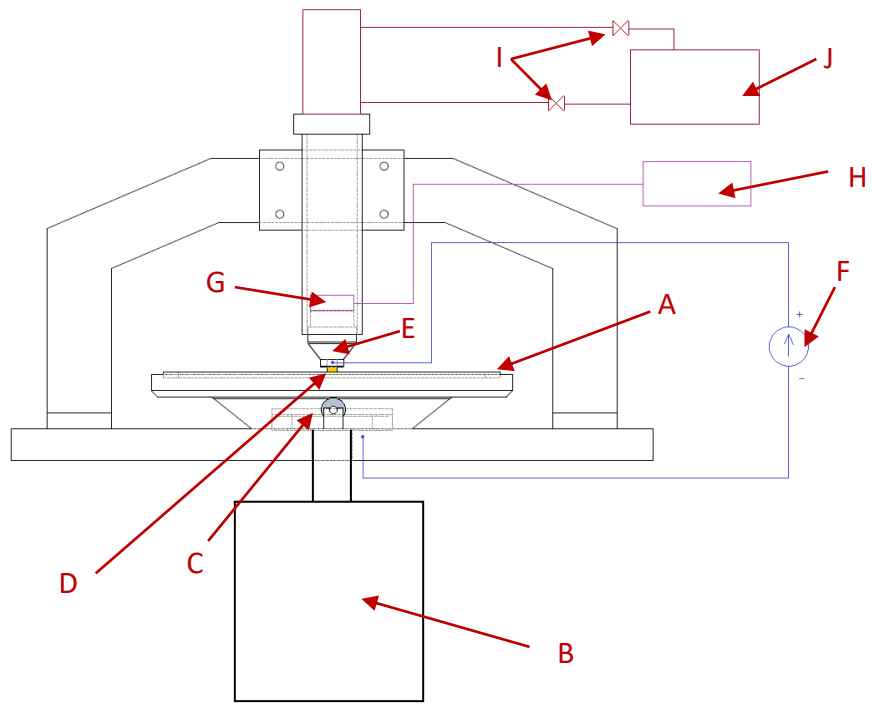


Fig. 1. Schematic diagram of pin-on-disc tribometer: (A) rotating disc; (B) high speed motor; (C) bearing support; (D) specimen; (E) specimen holder; (F) power supply; (G) force sensor; (H) manometer; (I) oil control valves; (J) oil pressure pump and tank.

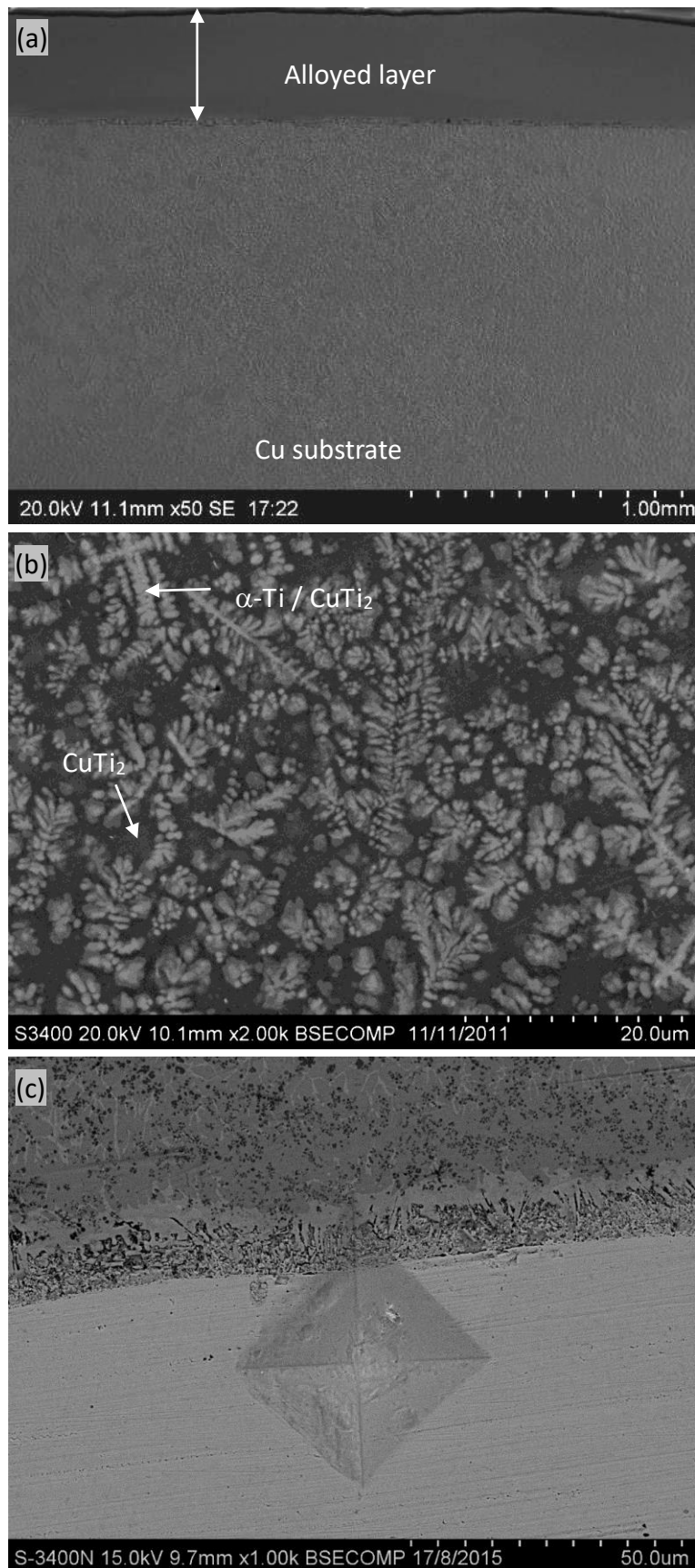
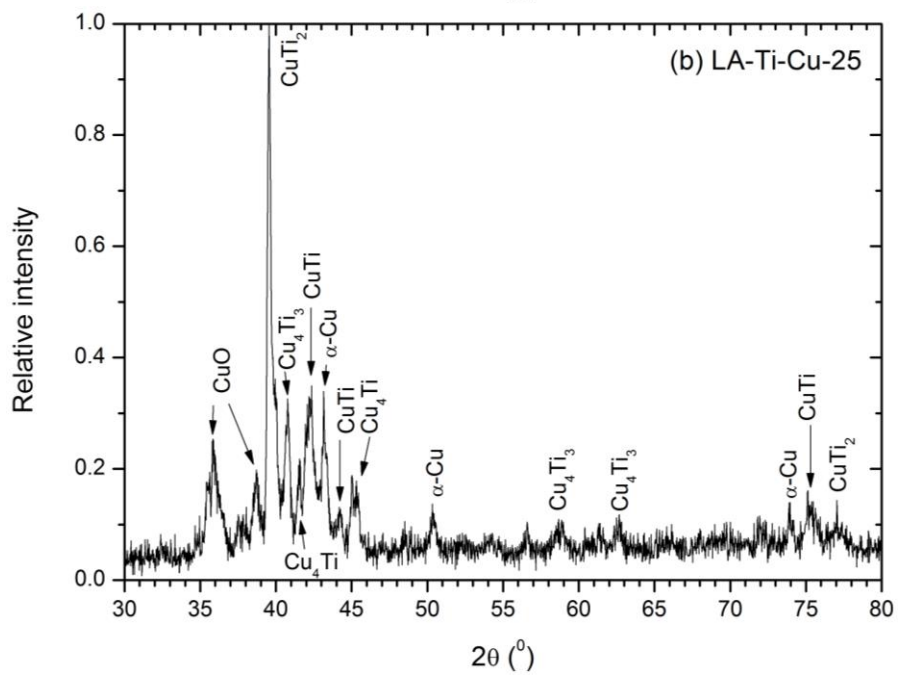
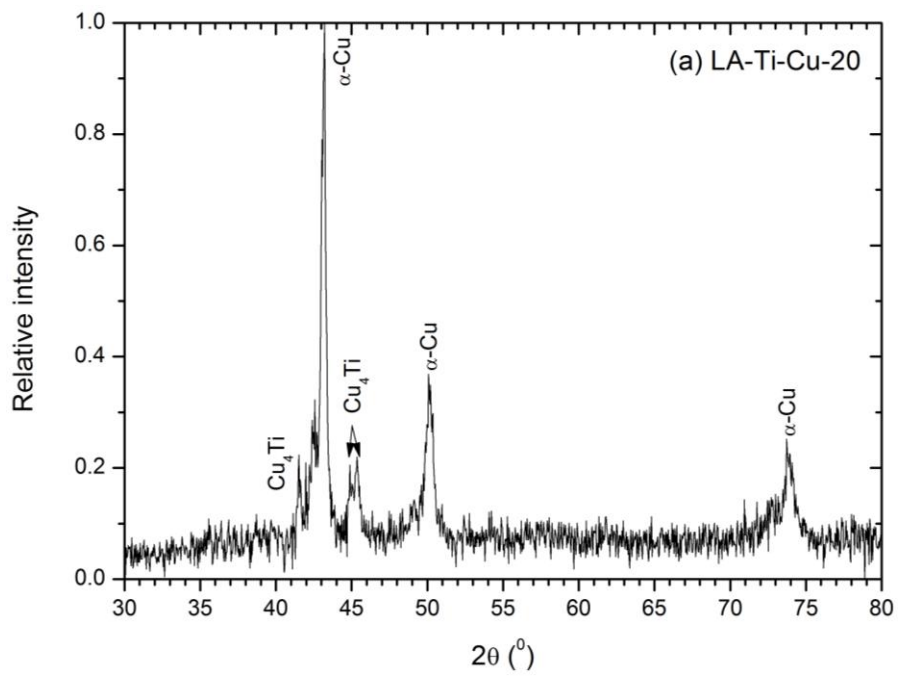


Fig. 2. Laser-allyed specimen fabricated at scanning speed of 30 mm/s (LA-Ti-Cu-30) showing: (a) cross-sectional view, (b) microstructures and (c) interface between the alloyed layer and substrate.



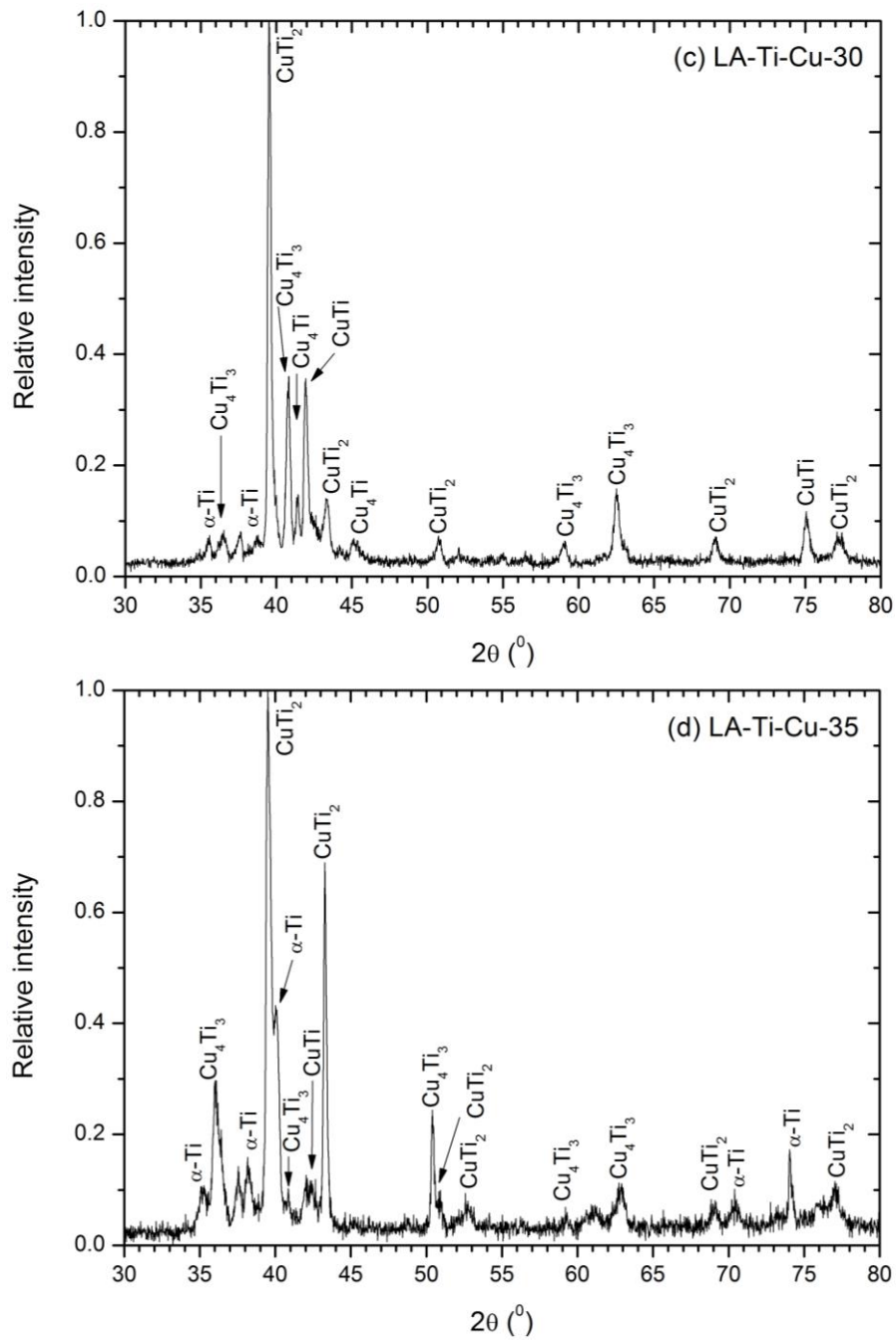


Fig. 3. XRD patterns of laser-alloyed specimens fabricated at scanning speeds of (a) 20 mm/s, (b) 25 mm/s, (c) 30 mm/s and (d) 35 mm/s.

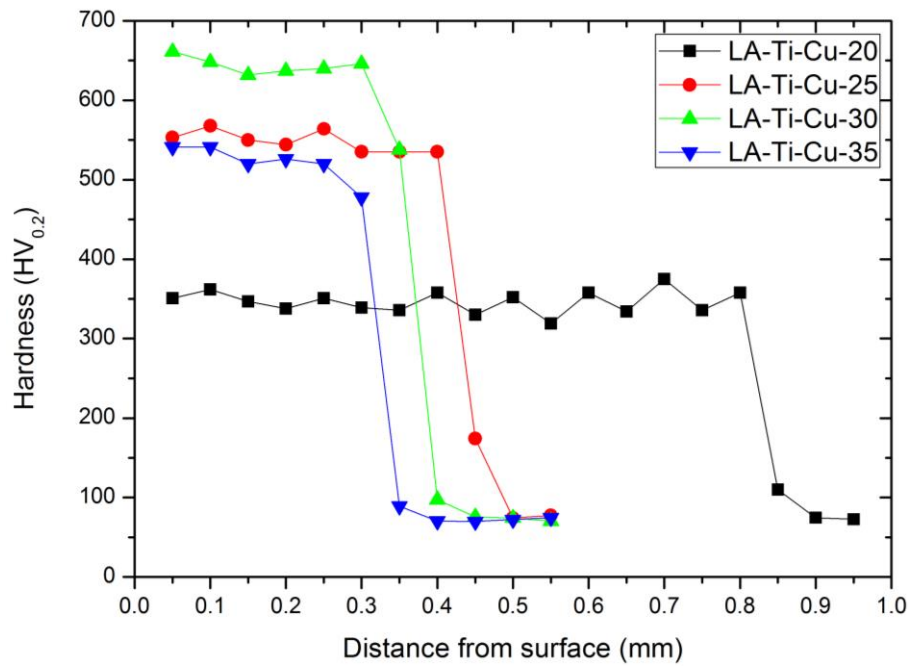


Fig. 4. Hardness profiles of various laser-alloyed samples.

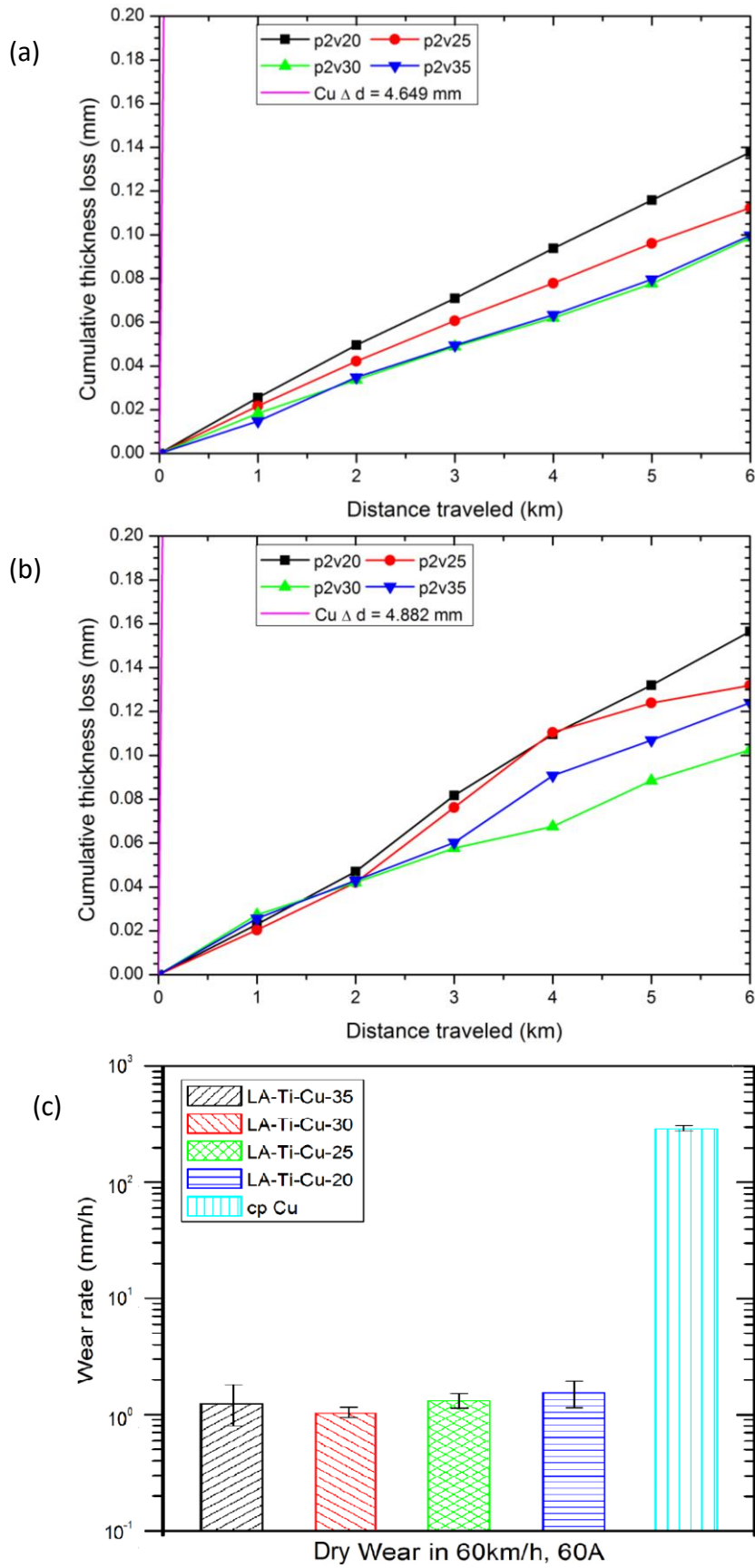


Fig. 5. Cumulative thickness loss against distance traveled for various specimens in dry wear at (a) 60 km/h, 0 A, (b) 60 km/h, 60 A and (c) electrical wear rates of cp Cu and various laser-alloyed samples.

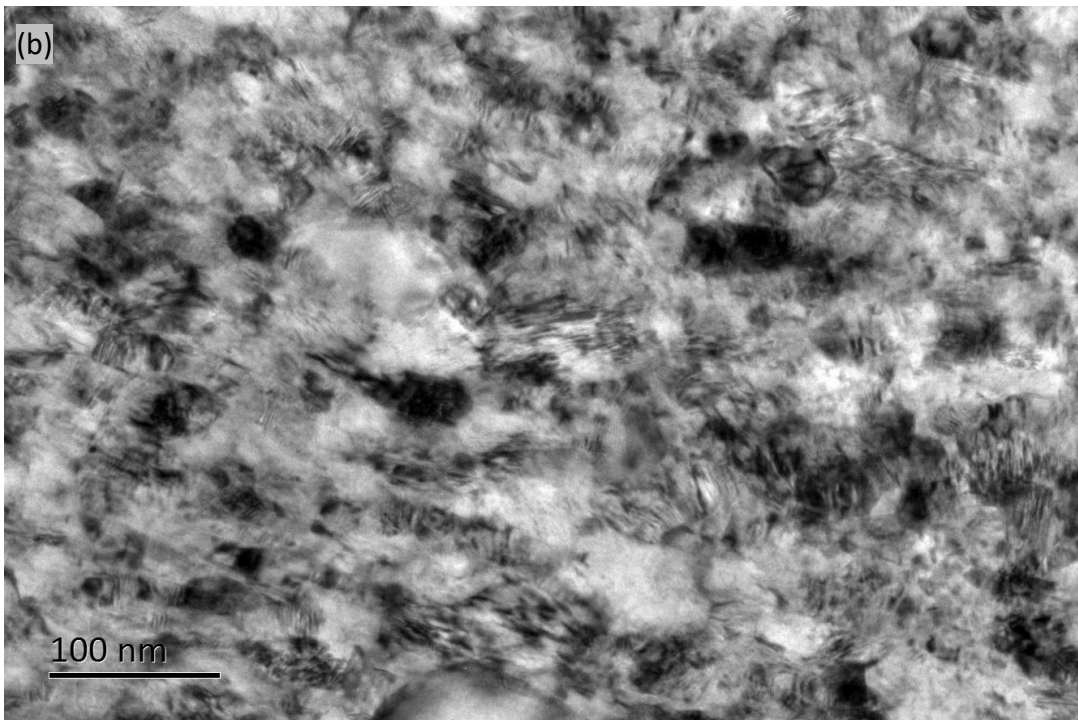
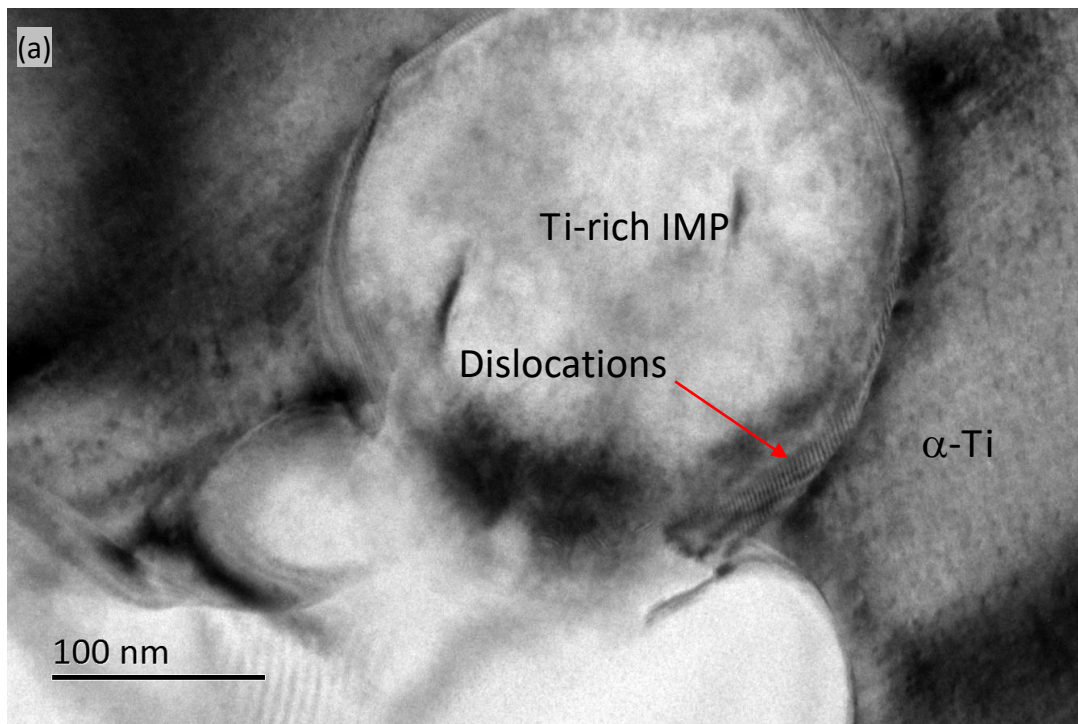


Fig. 6. TEM micrographs of LA-Ti-Cu-30 (a) before and (b) after electrical sliding wear at 60 km/h and 60 A, in dry condition.

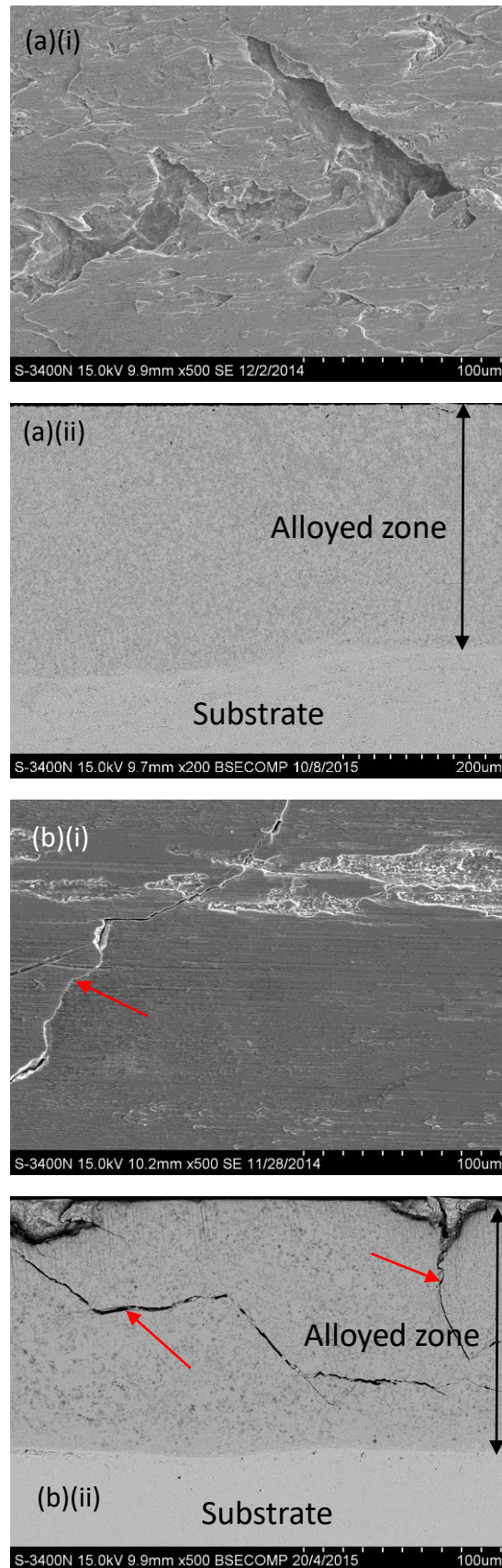


Fig. 7. Worn morphology of (a) LA-Ti-Cu-20 and (b) LA-Ti-Cu-30 at 60 km/h, 60A in air (i) surface view and (ii) cross-sectional view in dry conditions.

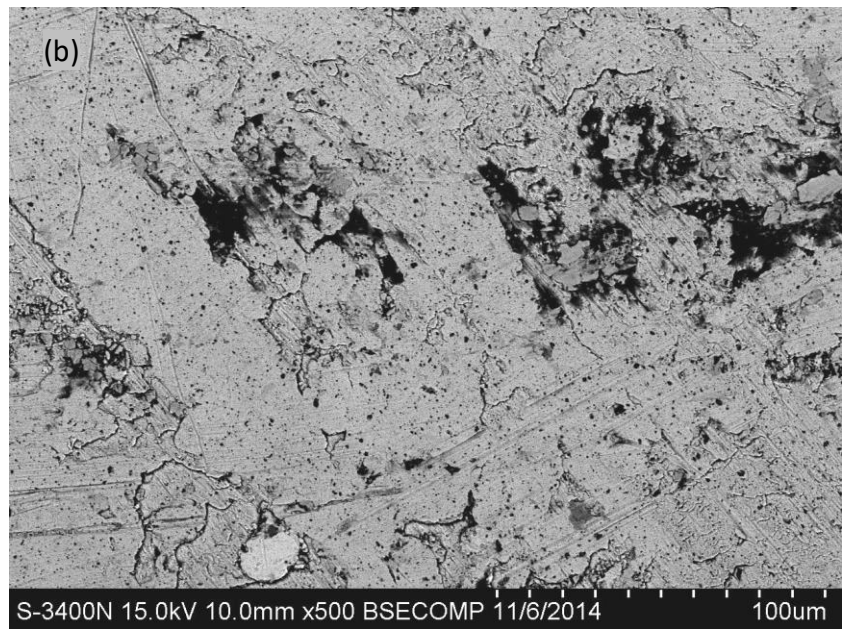
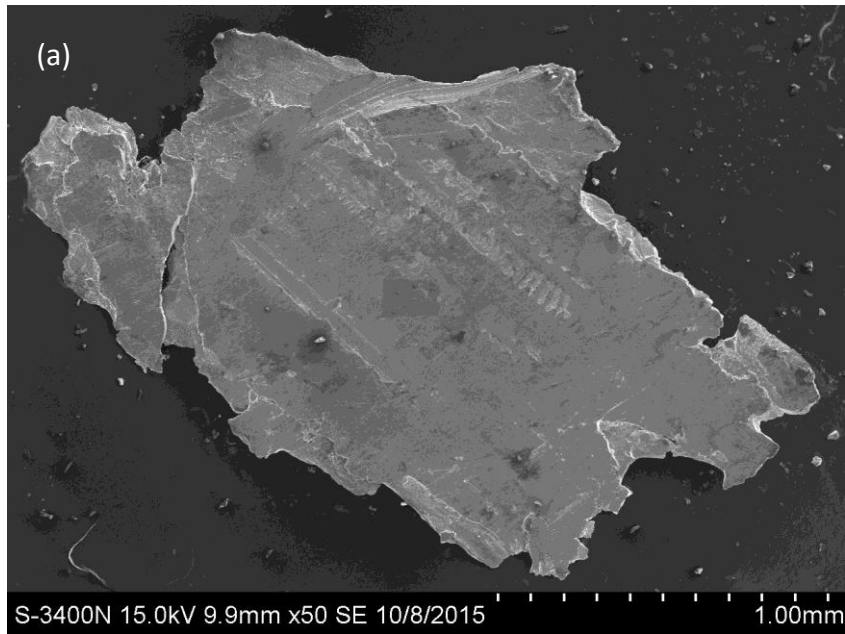


Fig. 8. Debris pulled out from LA-Ti-Cu-20 sliding at 60 km/h, 60 A in dry condition.

Part II

Legends of figures

Fig. 1. Schematic of the interfacial contact resistance measurement.

Fig. 2. (a) Plot of OCP vs time and (b) potentiodynamic polarization curves of various specimens in SAR at 25 °C.

Fig. 3. Morphologies of corroded surface of (a) LA-Ti-Cu-20 and (b) LA-Ti-Cu-30 after potentiodynamic polarization test in SAR at 25 °C.

Fig. 4. Cumulative thickness loss against distance traveled for various specimens in (a) wet wear with distilled water (DW) and (b) wet wear with SAR: (i) 60 km/h, 0 A and (ii) 60 km/h, 60 A.

Fig. 5. Electrical wear rates of various laser-alloyed samples and cp Cu at 60 km/h, 60 A under different environmental conditions.

Fig. 6. Worn morphology of (a) LA-Ti-Cu-20 and (b) LA-Ti-Cu-30 at 60 km/h, 60A in SAR (i) surface view and (ii) cross-sectional view.

Fig. 7. Plot of *ICR* versus applied compression force for various specimens.

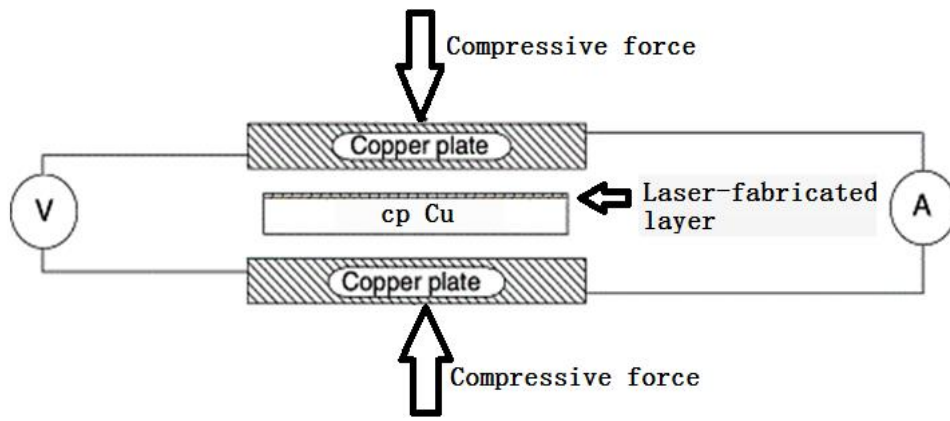
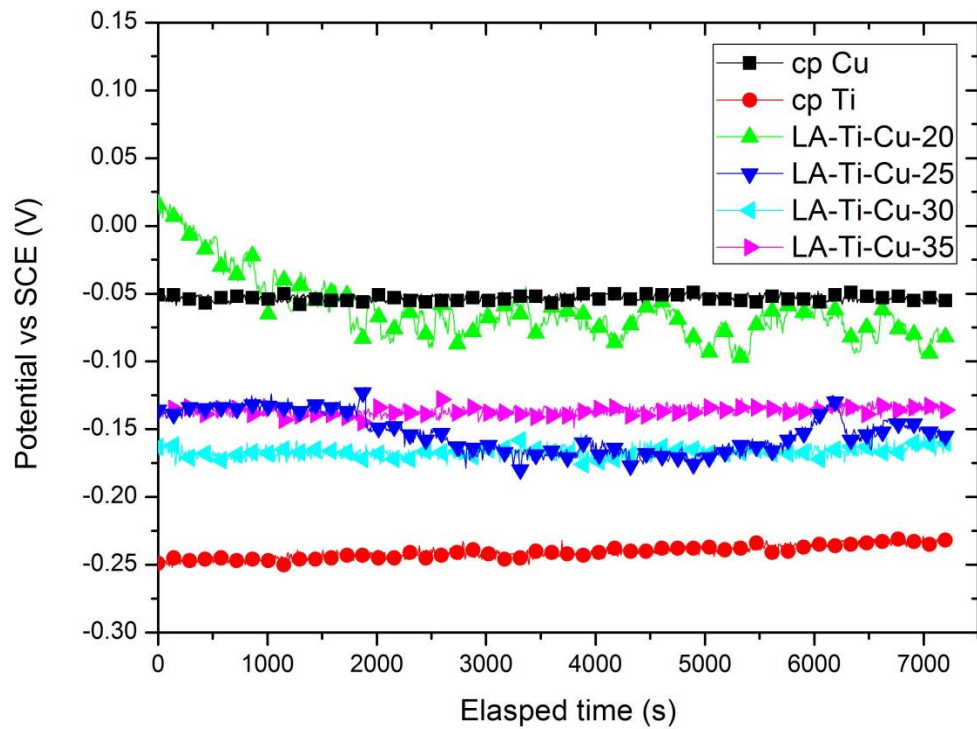
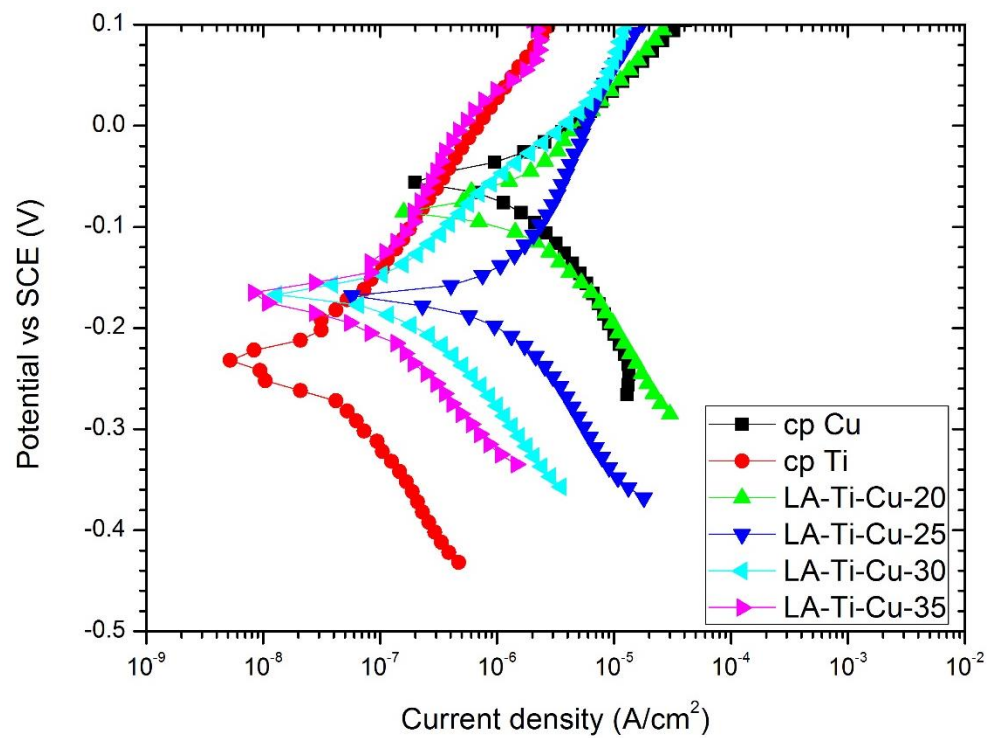


Fig. 1. Schematic of the interfacial contact resistance measurement.



(a)



(b)

Fig. 2. (a) Plot of OCP vs time and (b) potentiodynamic polarization curves of various specimens in SAR at 25 °C.

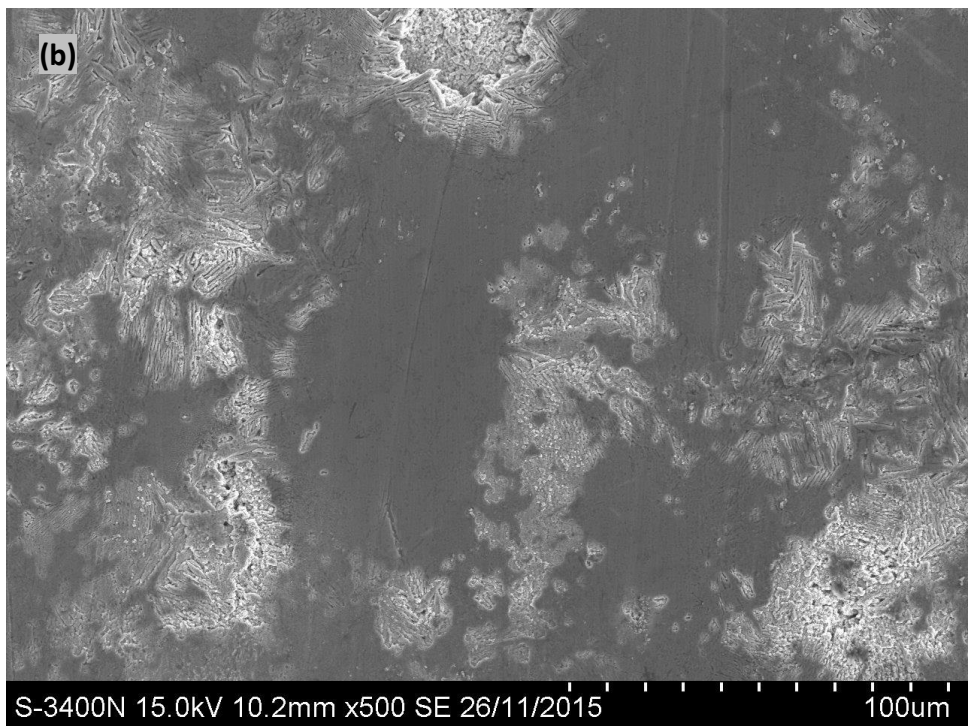
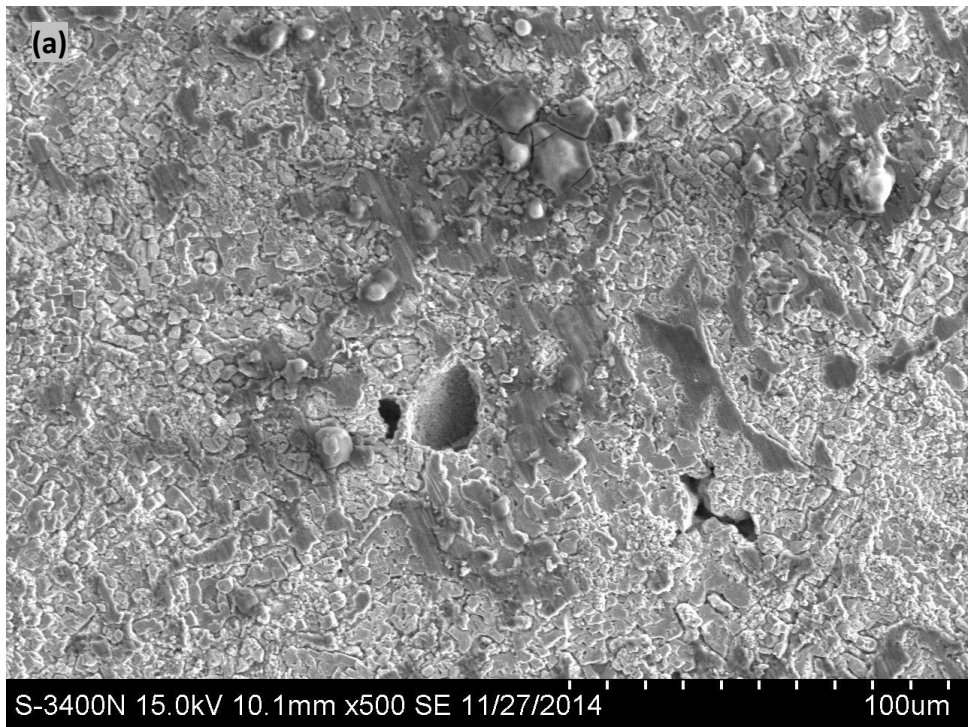


Fig. 3. Morphologies of corroded surface of (a) LA-Ti-Cu-20 and (b) LA-Ti-Cu-30 after potentiodynamic polarization test in SAR at 25 °C.

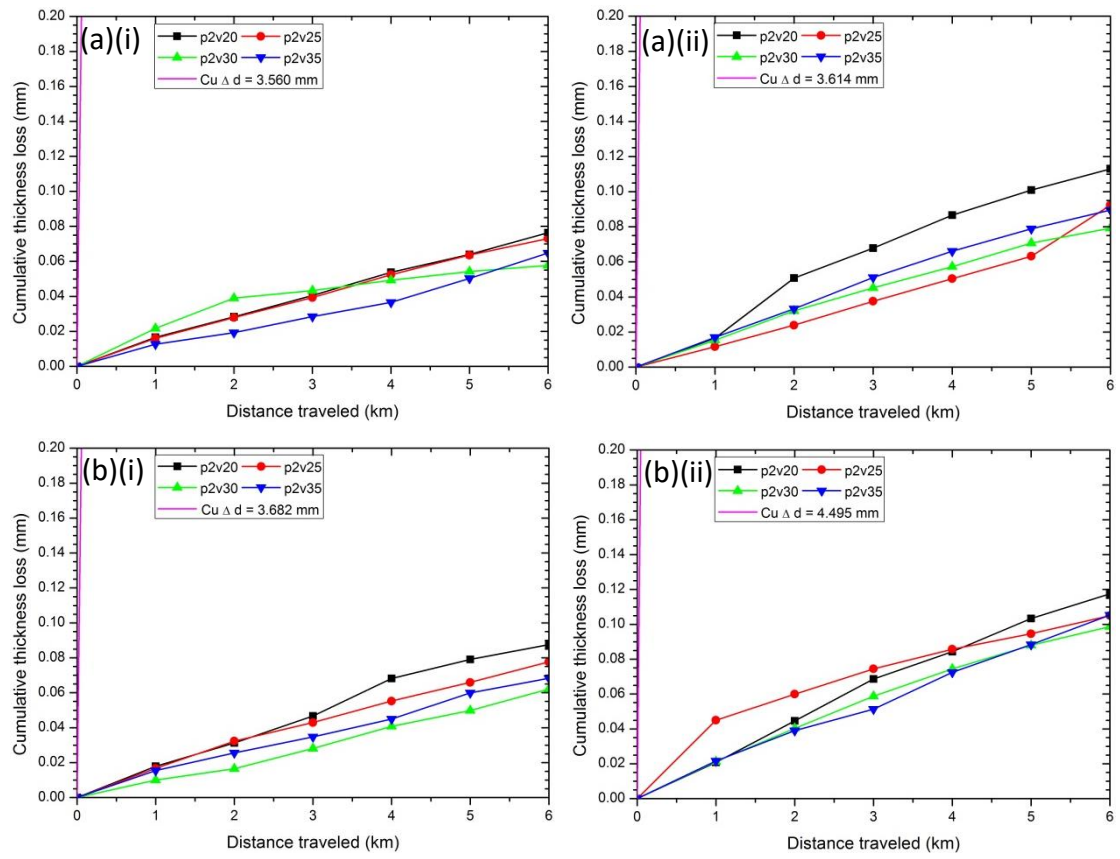


Fig. 4. Cumulative thickness loss against distance traveled for various specimens in (a) wet wear with distilled water (DW) and (b) wet wear with SAR: (i) 60 km/h, 0 A and (ii) 60 km/h, 60 A.

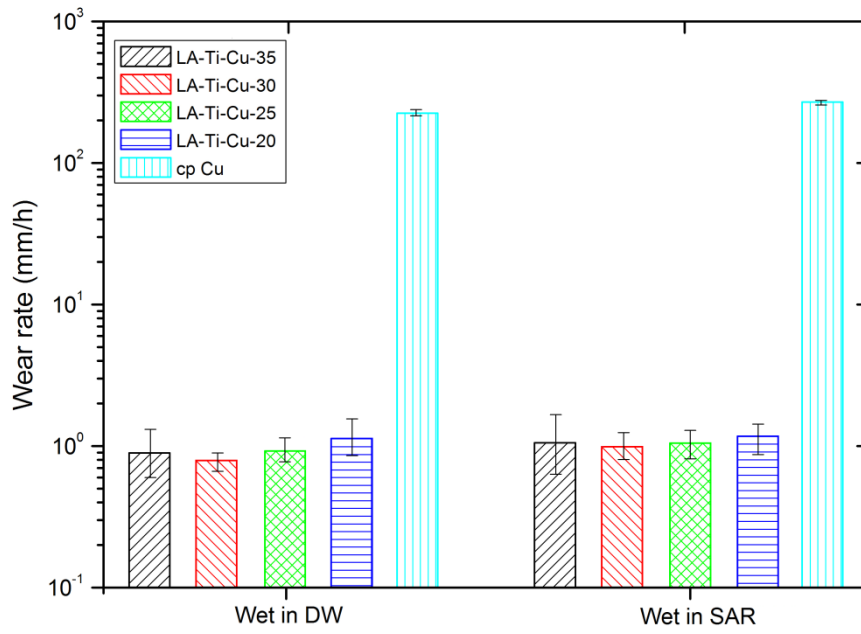


Fig. 5. Electrical wear rates of various laser-alloyed samples and cp Cu at 60 km/h, 60 A under different environmental conditions.

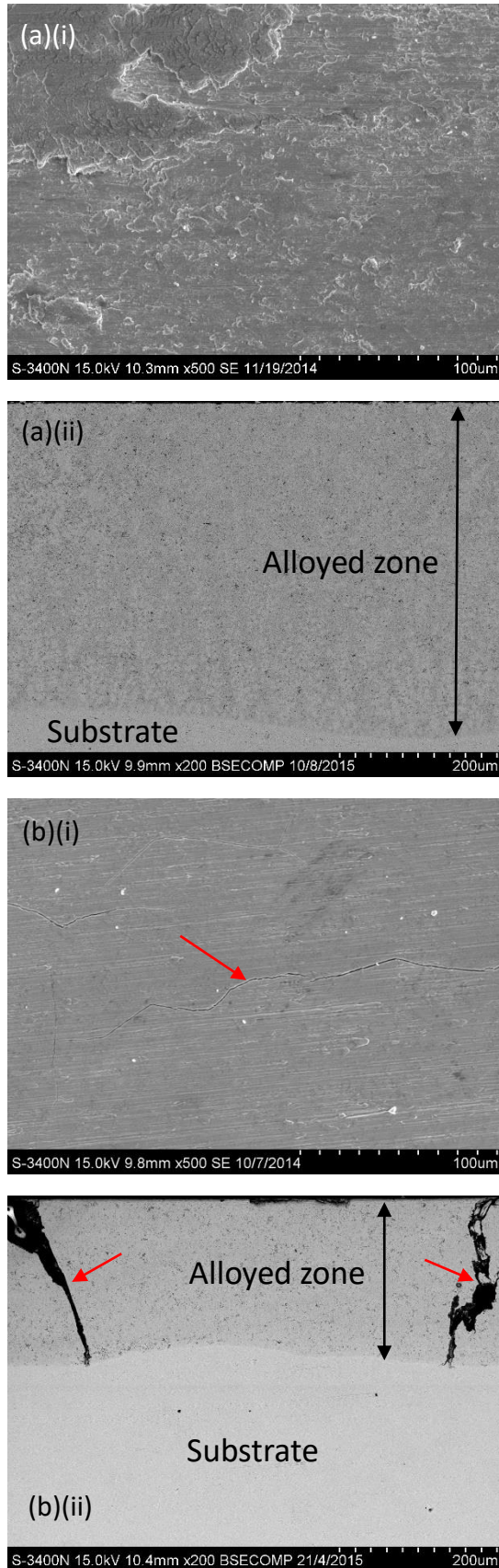


Fig. 6 Worn morphology of (a) LA-Ti-Cu-20 and (b) LA-Ti-Cu-30 at 60 km/h, 60A in SAR (i) surface view and (ii) cross-sectional view.

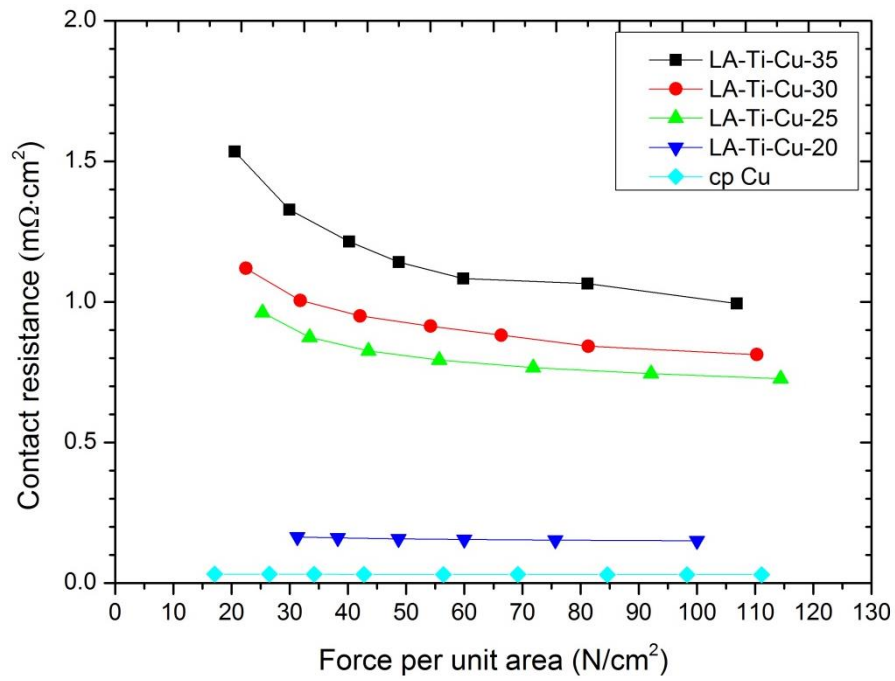


Fig. 7 Plot of *ICR* versus applied compression force for various specimens.